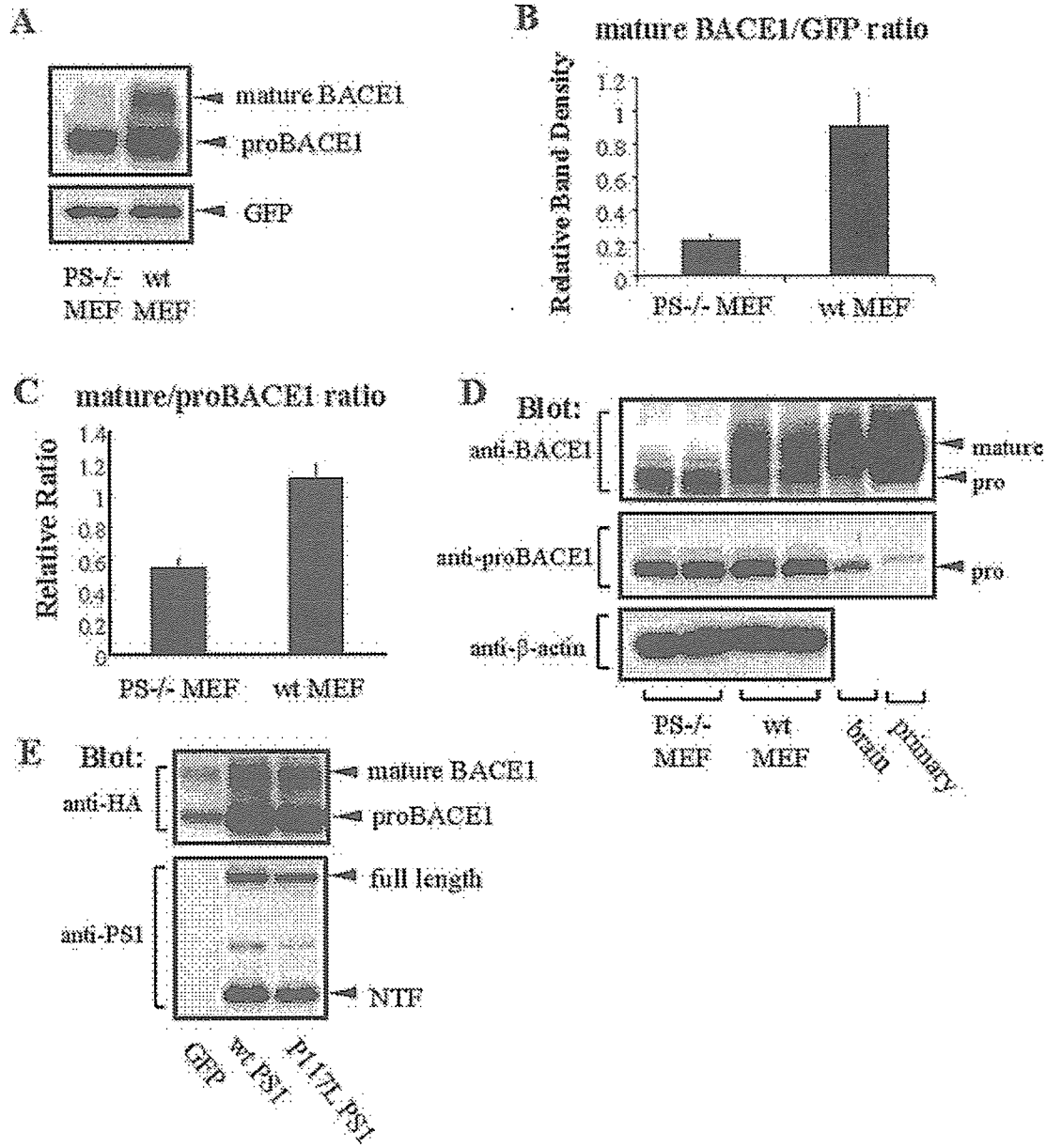

Fig. 1. PS1 is involved in BACE1 maturation post-translationally. **A:** HA-tagged BACE1 and GFP cDNA were transiently cotransfected into mouse embryonic fibroblasts (MEFs) derived from either wild-type (wt) or PS1/PS2 double-knockout (PS−/−) mice. Twenty-four hours after transfection, the cells were collected and each cell lysate was subjected to Western blot analysis and probed by either monoclonal anti-HA antibody or anti-GFP antibody. The level of mature BACE1 was apparently decreased in PS−/− MEFs as compared to that in wt MEFs, whereas the levels of GFP were almost similar between them. One representative immunoblot is shown. **B:** The band densities of either mature BACE1 or control GFP in four independent experiments were quantified by NIH imaging. The ratio of mature BACE1:GFP was calculated and analyzed by Student's *t*-test. The ratio of mature BACE1:GFP in PS−/− MEFs was significantly reduced, compared to that in wt MEFs ($n = 4$, $P < 0.0005$). **C:** The ratio of mature:proBACE1 was quantified by NIH imaging and analyzed by Student's *t*-test. The ratio of mature BACE1:proBACE1 in PS−/− MEFs was apparently reduced, compared to that in wt MEFs ($n = 4$, $P < 0.0005$). **D:** Equal amounts of cell lysates obtained from wt and PS−/− MEFs were subjected to Western blotting using the indicated antibodies. Lysates of mouse brain tissue and mouse primary neurons were used as positive controls. The endogenous level of mature BACE1 was drastically reduced in PS−/− MEFs as compared to those in wt MEFs, whereas the levels of proBACE1 were almost constant between them. One representative immunoblot is shown. **E:** Plasmids to encode either GFP, wt PS1, or P117L PS1 were cotransfected with HA-tagged BACE1 plasmid into PS−/− MEFs by 1:1 ratio. Each cell lysate was subjected to Western blotting analysis using the indicated antibodies. The levels of mature and proBACE1 were drastically increased in the cells expressing either wt PS1 or P117L PS1 as compared to those in the control cells. One representative immunoblot is shown.

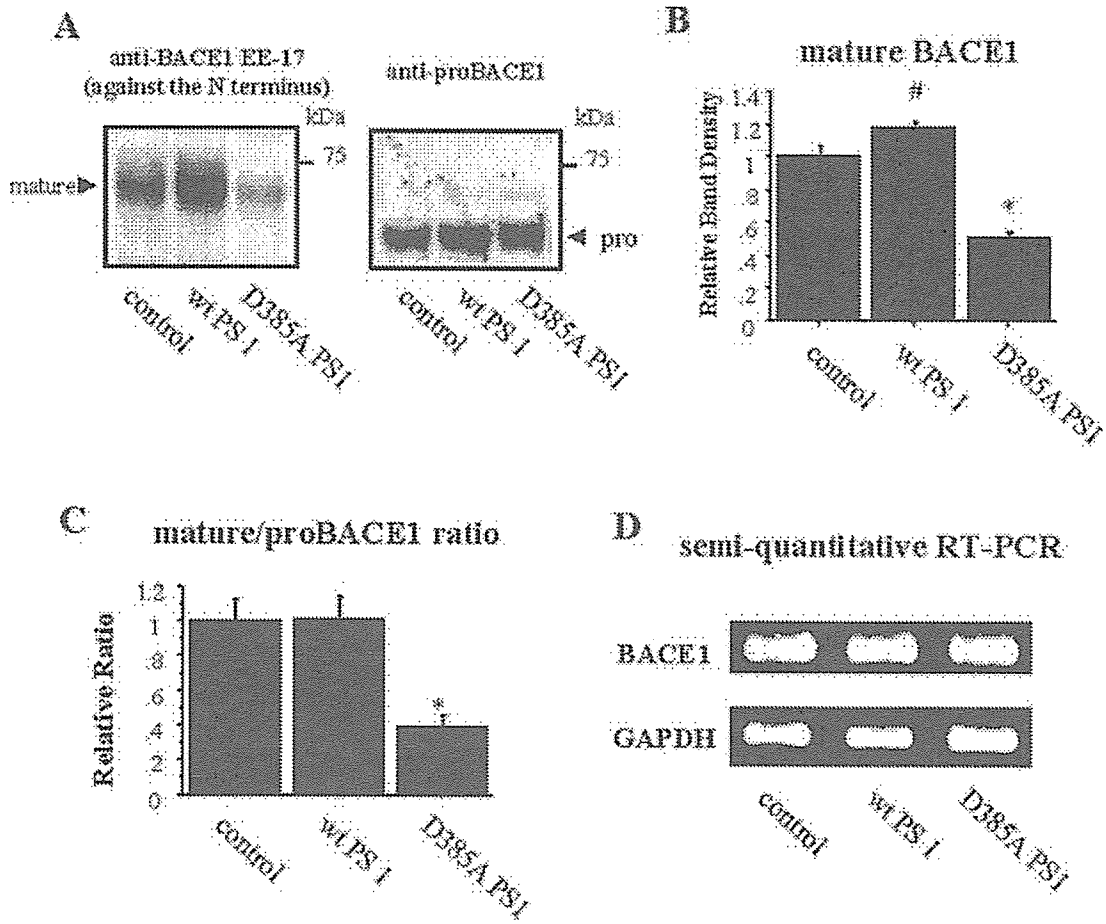

Fig. 2. **A:** Protein levels of BACE1 were compared between control SH-SY5Y cells and SH-SY5Y cells stably expressing either wt PS1 or D385A PS1. Equal amounts of whole cell lysates were subjected to Western blotting using the indicated antibodies. Mature BACE1 polypeptide was identified as a higher band of 70–75 kDa, whereas pro-BACE1 polypeptide was identified as a tighter band of 65 kDa. **B:** Immunoblotting of the mature BACE1 in each cell line was quantified by NIH imaging and analyzed by one-way ANOVA. The level of mature BACE1 was significantly reduced in D385A PS1 cells and increased in wt PS1 cells ($n = 3$, $^{\#}P < 0.01$ vs. control, $^{*}P < 0.0001$). **C:** The ratio of mature:proBACE1 in each cell line was quantified by NIH imaging and analyzed by one-way ANOVA. The ratio of mature: proBACE1 in D385A PS1 cells was significantly reduced ($n = 3$, $P < 0.001$ vs. control). **D:** The representative data of semi-quantitative RT-PCR analysis are shown. The processed cDNA was amplified by PCR using primers specific for either the human BACE1 gene or the human GAPDH gene. No significant differences in the levels of expression of BACE1 or GAPDH mRNA were observed among the cell lines.

(a 624-bp PCR product) and GAPDH mRNA (a 251-bp PCR product), a house keeping gene, were identified in these cell lines by RT-PCR analysis. The levels of BACE1 mRNA were comparable among these cell lines, whereas the levels of GAPDH mRNA were almost constant among them (Fig. 2D). Quantitative analysis, using GAPDH as an internal standard, showed that the levels of BACE1 mRNA expression were not statistically different among these cell lines (data not shown). These results indicate that the difference in BACE1 protein levels is not caused by a transcriptional regulation.

The above results suggest that wt PS1 significantly upregulates BACE1 maturation, presumably via facilitating the conversion of proBACE1 into mature BACE1 or stabilizing proBACE1. Conversely, PS deficiency and dominant-negative PS1 strongly downregulate it, indicating a novel role of PS1 for regulating BACE1 maturation.

Effect of γ-Secretase Inhibitors on BACE1 Maturation in Mouse Primary Neurons

To test whether PS1/γ-secretase activity directly affects the trafficking and maturation of BACE1 or not, we used two well-characterized γ-secretase inhibitors, L-685,458 and DAPT. Mouse primary neurons were treated with either 2 μM L-685,458, 1 μM DAPT or vehicle (DMSO) for 4 days. Equal amount of each cell lysate was subjected to Western blotting analysis using anri-BACE1 antibody (EE-17), anti-proBACE1 antibody, and anti-APP antibody (against the C terminus). As shown in Figure 3, we observed

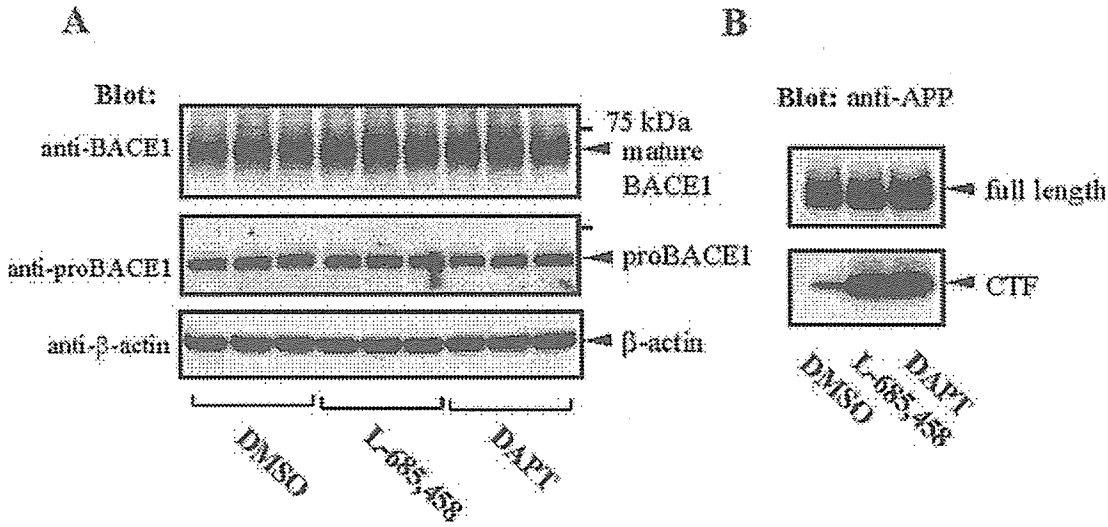

Fig. 3. Mouse primary neurons were treated with either 2 μM L-685,458, 1 μM DAPT or vehicle (DMSO) for 4 days. Equal amount of each cell lysate was subjected to Western blotting analysis using the indicated antibodies. No significant difference was seen in the levels of mature and proBACE1 between each treatment group (**A**), whereas APP CTF remarkably accumulated after each γ-secretase inhibitor, indicating that γ-secretase activity was effectively inhibited (**B**). One representative immunoblot is shown.

no significant difference in the levels of mature and pro-BACE1 between each treatment group (left panel), whereas APP C-terminal fragment remarkably accumulated after L-685,458 or DAPT treatment, indicating that γ-secretase activity was effectively inhibited (right panel). Thus, we consider that PS1/γ-secretase activity itself is less likely to be involved in the maturation process of BACE1.

PS1 and BACE1 Immunoprecipitation in the Cell and the Brain Tissue

A recent report showed that PS1 directly interacts with BACE1 in double transfected human embryonic kidney 293T cells (Hebert et al., 2003). We investigated whether wt PS1 and/or D385A PS1 can be associated with BACE1 in our experimental system. To answer this question, HA-tagged BACE1 and either wt PS1 or D385A PS1 were transiently co-expressed in PS−/− MEFs. The cells were harvested about 24 hr after transfection, and equal amounts of each cell lysate was immunoprecipitated using the anti-PS1 antibody against the N terminus, followed by the Western blot analysis using monoclonal anti-HA antibody. As shown in Figure 4A, wt (lane 1) and D385A PS1 (lane 2) were apparently associated with proBACE1 but not mature BACE1 in the transfected cells.

Next, we extended our findings obtained from the analysis of MEF cells to the SH-SY5Y cell lines. Equal amounts of cell lysate obtained from each cell line were immunoprecipitated using the anti-BACE1 antibody (targeting amino acids 487–501; Calbiochem). The cell lysates (Lys) as well as the immunoprecipitates (IP) were then subjected to Western blotting using the MAB5232 antibody (against the loop domain of PS1). As shown in Figure 4B, more PS1 C-terminal fragment (CTF) immunoreactivity was observed in wt PS1 cells (lane 7) than in control cells (lane 6), whereas almost no PS1 CTF bound to BACE1 was detected in D385A PS1 cells (lane 8; lower panel), reflecting the diminished endoproteolysis of D385A PS1 (lane 3). Conversely, solid association between the full-length D385A PS1 and BACE1 was observed (Fig. 4B, lane 8; upper panel). Furthermore, we showed the in vivo interaction between PS1 CTF and BACE1, using adult mouse brain tissue (Fig. 4C). The above results indicate that PS1 is preferably bound to proBACE1 rather than mature BACE1 and the functional binding can be contributed to the maturation of BACE1.

PS1 and BACE1 Colocalization in the SH-SY5Y Cells and Primary Neurons

To support the interaction between PS1 and BACE1 obtained from the immunoprecipitation experiment, we examined the intracellular localization of these two biochemical partners by immunofluorescent confocal microscopy, using control, wt PS1, and D385A PS1 SH-SY5Y cells. After permeabilization, cells were doubly stained with the antibody MAB5308 to visualize BACE1 and the anti-PS1 antibody (against the N terminus) to visualize PS1. As shown in Figure 5A–C, the PS1 in each cell line largely colocalized with the endogenous BACE1. Consistent with the above result shown in Figure 2A, an increase in wt PS1 immunoreactivity was apparently accompanied by an increase in endogenous BACE1 immunoreactivity (Fig. 5B, compared to 5A).

To further confirm the colocalization of PS1 and BACE1 in physiologically relevant system, endogenous PS1 and BACE1 were doubly immunostained in rat primary cultured cortical neurons at 5 days in vitro, using

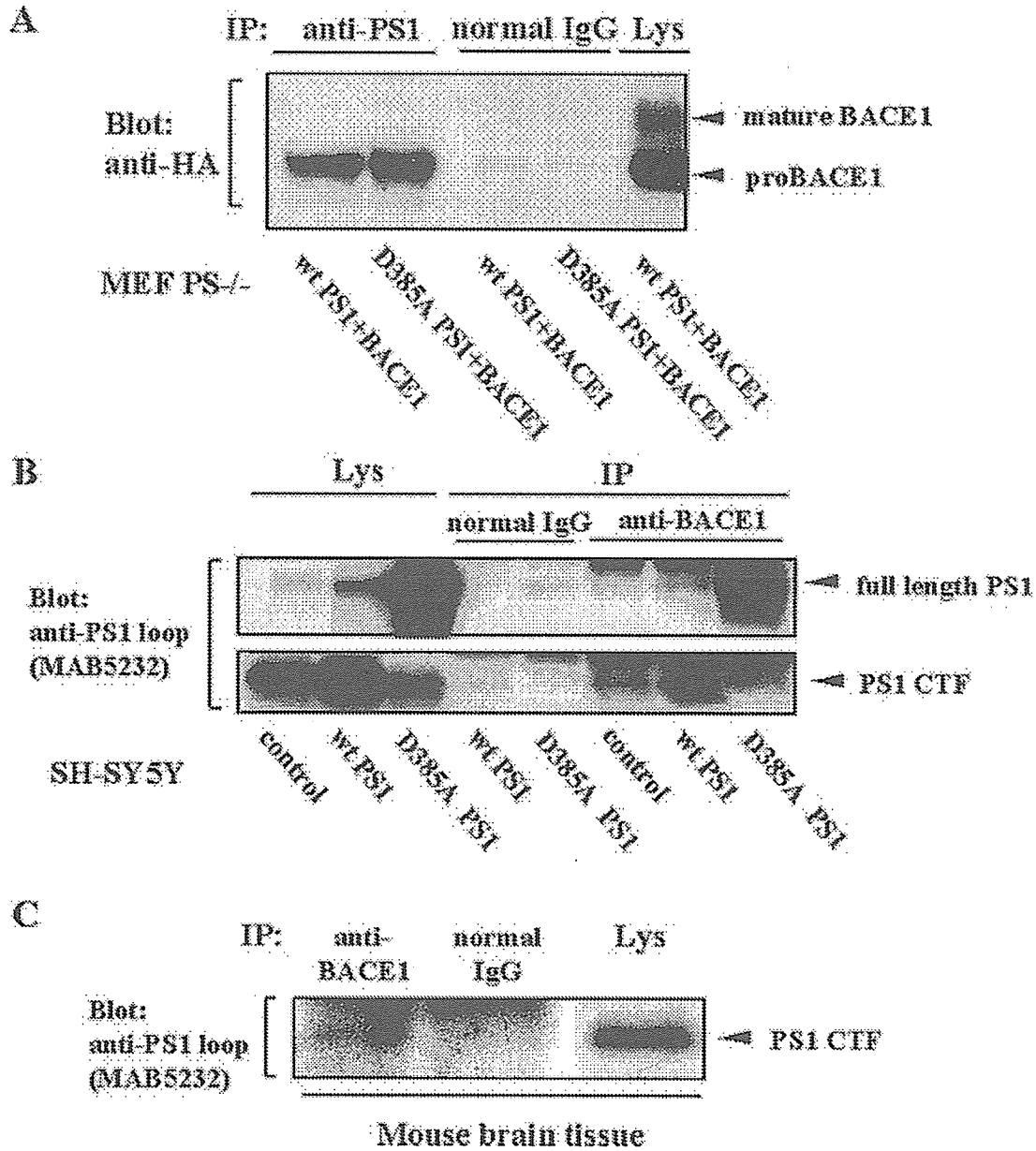

Fig. 4. PS1 and BACE1 physically interact with each other. **A:** HA-tagged BACE1 and either wt PS1 or D385A PS1 were transiently cotransfected into PS−/− MEFs. Each cell lysate was immunoprecipitated with anti-PS1 antibody against the N terminus. The cell lysate (Lys) as well as the immunoprecipitates (IP) were subjected to Western blotting with anti-HA antibody. ProBACE1, but not mature BACE1, was co-immunoprecipitated with either wt PS1 or D385A PS1. Almost no BACE1 immunoreactivity was observed from the samples of normal rabbit IgG used as negative controls. **B:** Equal amounts of cell lysates obtained from each SH-SY5Y cell line were immunoprecipitated using the anti-BACE1 antibody against the C terminus (Calbiochem), followed by Western blotting with the MAB5232 antibody against the loop domain of PS1. More PS1 C-terminal fragment (CTF) immunoreactivity was detected in wt PS1 cells (lane 4) than in control cells (lane 5). In D385A PS1 cells, almost no PS1 CTF bound to BACE1 was observed (lane 8: lower panel), reflecting the diminished endoproteolysis of D385A PS1 (lane 3). Conversely, solid association between full-length D385A PS1 and BACE1 was observed (lane 8: upper panel). Note that full-length wt PS1 was also associated with BACE1 in wt PS1 cells (lane 8: upper panel). No PS1 immunoreactivity was observed from the samples of normal rabbit IgG used as negative controls (lanes 5,6). **C:** Equal amounts of cell lysates obtained from adult mouse brain tissue were immunoprecipitated using the anti-BACE1 antibody (Calbiochem), followed by Western blotting using the MAB5232 antibody against the loop domain of PS1. PS1 CTF immunoreactivity was detected in the immunoprecipitates with the anti-BACE1 antibody (Calbiochem), whereas no PS1 CTF immunoreactivity was observed in the samples with normal rabbit IgG.

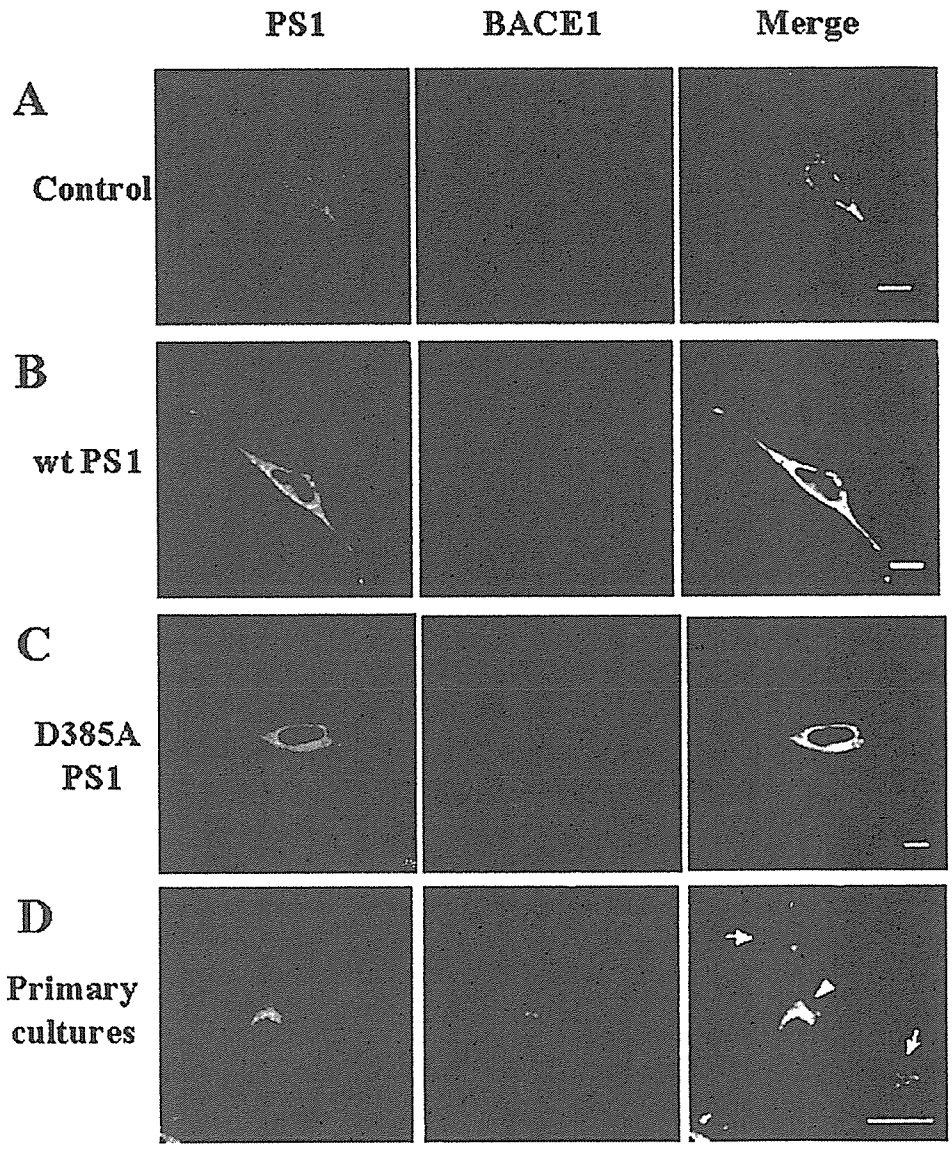

Fig. 5. PS1 and BACE1 colocalization in the SH-SY5Y cells and primary neurons. Each SH-SY5Y cell line (**A–C**) and rat primary cultured cortical neurons (**D**) were doubly stained with anti-BACE1 antibody against the C terminus (MAB5308) and anti-PS1 antibody against the N terminus. In each SH-SY5Y cell line, PS1 was largely colocalized with endogenous BACE1 (A–C, merged images). Note that an increase in wt PS1 immunoreactivity was accompanied by an increase in endogenous BACE1 immunoreactivity (A,B). Endogenous PS1 and BACE1 were considerably colocalized in a primary neuron, especially in a perinuclear area (arrowhead), compared to glial cells (arrows) (D, merged image). Scale bar = 20 μm.

anti-PS1 antibody against the N terminus and the MAB5308 antibody. As shown in Figure 5D, endogenous PS1 and BACE1 were considerably colocalized in a primary neuron, especially in a perinuclear area (arrowhead), compared to glial cells (arrows).

BACE1 in D385A PS1 Cells Fails to be Properly Transported From the ER to the Golgi

As shown in Figures 4 and 5, D385A PS1 is associated with endogenous BACE1 as well as wt PS1 in the immunoprecipitation and immunofluorescent experiments. However, BACE1 maturation is markedly downregulated in D385A PS1 cells in contrast to in wt PS1 cells (Fig. 2C). Because BACE1 undergoes trafficking-dependent maturation through the secretory pathway from the ER to the Golgi, we hypothesized that the transport of endogenous BACE1 from the ER to the Golgi was suppressed significantly in D385A PS1 cells. We first examined the intracellular localization of BACE1 in wt and D385A PS1 cells by immunofluorescent study using markers specific for the ER and the Golgi. Each cell line was double stained with the MAB5308 antibody to visualize BACE1 and either the anti-calnexin antibody to visualize the ER or the anti-mannosidase II antibody to visualize the Golgi. Interestingly, we found that a part of BACE1 in wt PS1 cells was apparently colocalized with mannosidase II in the perinuclear area (Fig. 6A, arrowhead), whereas the colocalization was negligible in D385A PS1 cells (Fig. 6B). Moreover, in D385A PS1 cells, most of BACE1 was colocalized with calnexin, a marker for the ER (Fig. 6C). These results suggest that proper transport of BACE1 from the ER to the

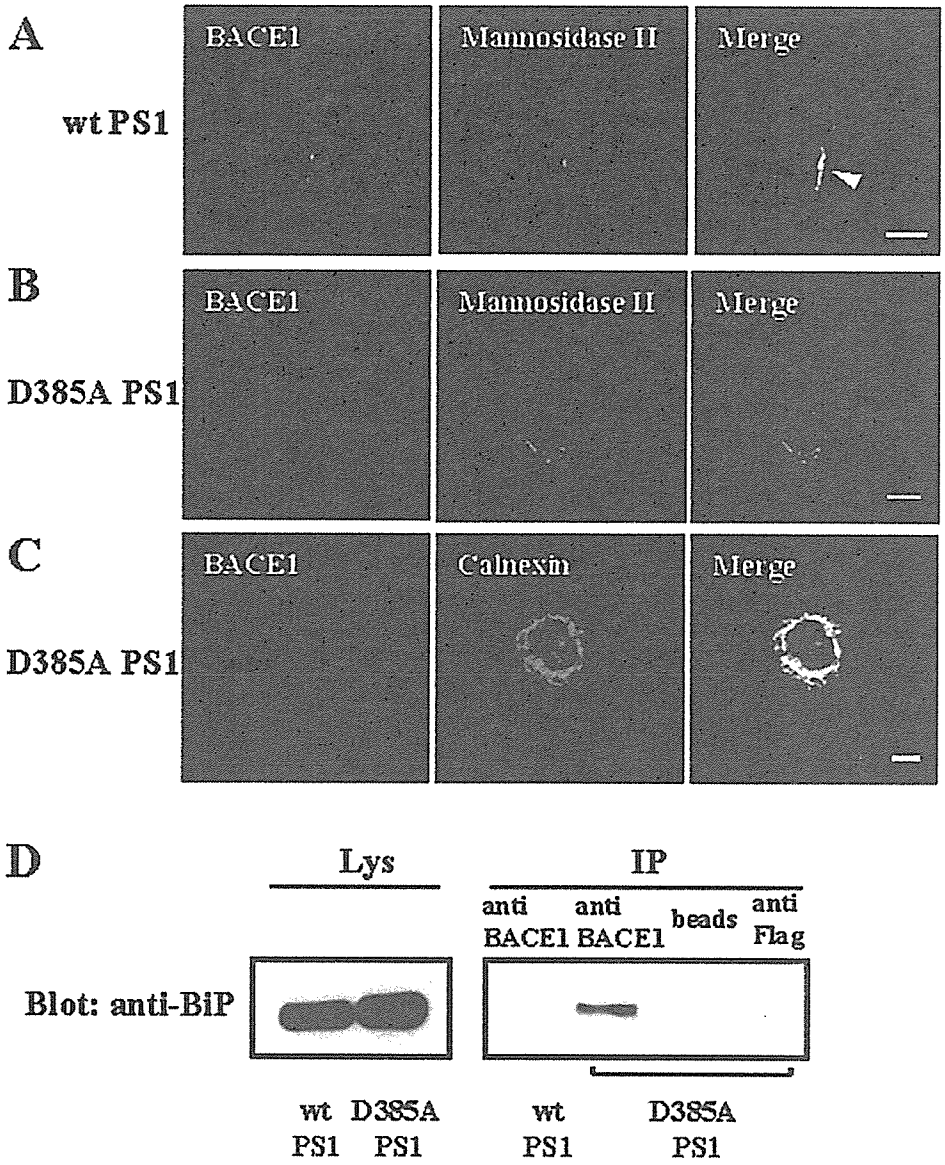

Fig. 6. Endogenous BACE1 in D385A PS1 cells is largely retained in the ER and fails to be transported to the Golgi. **A,B:** Wt PS1 cells and D385A PS1 cells were doubly stained with anti-BACE1 antibody against the C terminus (MAB5308) and anti-mannosidase II antibody. No apparent colocalization of endogenous BACE1 with mannosidase II, a marker for the Golgi, was observed in D385A PS1 cells (B), whereas endogenous BACE1 in wt PS1 cells was partially colocalized with mannosidase II (A, arrowhead). **C:** D385A PS1 cells were doubly stained with anti-BACE1 antibody (MAB5308) and anti-calnexin antibody. Endogenous BACE1 in D385A PS1 cells was colocalized mostly with calnexin, a marker for the ER (C, merged image). Scale bar = 20 μm. **D:** Equal amounts of whole cell lysates from wt PS1 and D385A PS1 cells were immunoprecipitated with anti-BACE1 antibody (MAB5308). Cell lysate (Lys) as well as immunoprecipitates (IP) were subjected to immunoblotting with anti-BiP antibody. The immunoprecipitates from D385A PS1 cell lysate showed BiP immunoreactivity. No BiP immunoreactivity was observed in the immunoprecipitate from the wt PS1 cell lysate, or from the samples of Protein G-Sepharose beads alone (beads) or anti-Flag antibody, used as negative controls.

Golgi is impaired in D385A PS1 cells, and are compatible with the previous observation that BACE1 maturation is downregulated in D385A PS1 (Fig. 2C).

BiP, an ER-resident molecular chaperone, binds to misfolded, underglycosylated, or unassembled proteins and assists with protein folding and retention of misfolded proteins in the ER (Gething, 1999). We examined the possibility that BACE1 in D385A PS1 cells, which might become terminally misfolded after release from the ER folding machinery, was preferentially associated with BiP. Equal amounts of cell lysate obtained from either wt PS1 or D385A PS1 cells were immunoprecipitated using the MAB5308 antibody, and the immunoprecipitate was subjected to Western blotting using an anti-BiP antibody. The immunoreactivity of BiP co-immunoprecipitated with BACE1 was observed in D385A PS1 cells, whereas it was not detected in wt PS1 cells (Fig. 6D).

These results suggest that proper transport of endogenous BACE1 from the ER to the Golgi is impaired in D385A PS1 cells, resulting in aberrant retention of BACE1 within the ER, and its association with BiP as unfolded or misfolded proteins.

DISCUSSION

Despite of extensive research, the pathogenesis of AD is still in an enigma. Several recent reports showed elevated β-secretase expression and enzymatic activity in the absence of the alteration of message expression in AD brains (Fukumoto et al., 2002; Holsinger et al., 2002; Yang et al., 2003), indicating the dysregulation of β-secretase activity may be involved in AD pathogenesis. Interestingly, amino-terminally truncated Aβ peptides, which are known to be β-secretase cleavage products, were more abundant in

the brains of subjects carrying PS1 gene mutations causing FAD than in those with sporadic AD and FAD associated with a point mutation in APP gene (Russo et al., 2000), indicating that FAD-linked mutations in PS1 can somehow affect β-secretase activity. However, the functional link between PS1 and BACE1 has never been elucidated, although they are supposed to be the 'key players' of AD pathogenesis.

In the present study, we showed a solid evidence for a novel function of PS1 in regulating BACE1 maturation. The levels of mature BACE1 either endogenously or exogenously expressed in PS−/− MEFs were reduced significantly, as compared to that in wt MEFs. These results suggest that the presence of presenilins can promote BACE1 maturation. To validate this effect of PS1 in neuronal cells endogenously expressing BACE1, we analyzed stably transfected SH-SY5Y cells with either wt PS1 or dominant-negative (D385A) PS1. Interestingly, the overexpression of D385A PS1 decreased the level of mature BACE1 protein by 50%, accompanied by a 60% reduction in the ratio of mature:proBACE1 as compared to control cells. Conversely, the overexpression of wt PS1 upregulated the level of mature BACE1 protein. Given that the levels of BACE1 mRNA were comparable between wt PS1 and D385A PS1 cells, these results indicate that functional PS1 positively regulates BACE1 maturation post-translationally.

Intriguingly, a recent study showed that targeting BACE1 to lipid rafts, cholesterol- and sphingolipid-enriched microdomains within cellular membranes, upregulated the β-site processing of APP, leading to a drastic increase in Aβ generation in SH-SY5Y cells (Cordy et al., 2003), indicating that proper distribution of BACE1 is crucially important for regulating Aβ generation. Although a growing number of evidence has strongly supported a direct role for PS1 in the γ-secretase cleavage of APP as the catalytic component of the γ-secretase complex (Wolfe et al., 1999a,b), a function of PS1 in protein trafficking has also been shown, especially with regard to APP and nicastrin (Kim et al., 2001; Edbauer et al., 2002; Leem et al., 2002a,b; Cai et al., 2003; Herreman et al., 2003). This function is consistent with a functional analogy to the weakly homologous SPE4 protein of *C. elegans*, which has been implicated in the maintenance of a Golgi-derived membranous organelle and is thought to be important in the partitioning of protein and cell membrane products in maturing spermatocytes (L'Hernault and Arduengo, 1992). These previous findings provide support for the idea that PS1 may regulate BACE1 trafficking, thereby modulating its maturation.

Indeed, we found that BACE1 in D385A PS1 cells was mostly retained within the ER and was negligibly localized within the Golgi (Fig. 6B,C), whereas a part of BACE1 in wt PS1 cells was apparently localized within the Golgi (Fig. 6A). Moreover, we found that BACE1 in D385A PS1 cells was associated significantly with BiP, an ER resident molecular chaperone, in contrast to in wt PS1 cells (Fig. 6D), presumably attributable to its aberrant retention within the ER. Interestingly, a splice variant of BACE1, lacking terminal two-thirds of exon 3, is expressed in pancreas. This isoform of BACE1, lacking β-secretase activity, colocalizes with BiP and its transport along the secretory pathway is blocked at the level of the ER, indicating that misfolded or non-functional BACE1 can associate with BiP in the ER (Bodendorf et al., 2001). These results indicate that wt PS1 upregulates BACE1 maturation, whereas the absence of PS1 or non-functional D385A PS1 downregulates its maturation as a result of its inefficient transport from the ER to the Golgi.

The above data raises the question whether PS1/γ-secretase activity directly affects the trafficking and maturation of BACE1 or not. We observed no significant effect of the γ-secretase inhibitors on BACE1 maturation in primary neurons. Thus, we consider that PS1/γ-secretase activity itself is less likely to be involved in the maturation process of BACE1. Nevertheless, further experiments will be needed to elucidate a relationship between the PS1/γ-secretase activity and the novel function of PS1 in the trafficking and maturation of BACE1.

Finally, how dose PS1 regulate BACE1 trafficking and maturation? Although this question was not clarified in the present study, it was reported recently that PS1 and BACE1 are transported in the same membrane vesicles along the axons *in vivo*, via the direct binding of APP to the kinesin light chain subunit of kinesin-I, a microtubule motor protein (Kamal et al., 2001). Moreover, it was also shown that PS1 and nicastrin, the major components of the γ-secretase complex, interact with BACE1, suggesting that they may regulate β-secretase activity via the interaction with BACE1 (Hattori et al., 2002; Hebert et al., 2003). Consistent with these reports, we showed PS1-BACE1 interaction in the cell lines, primary neurons, and brain tissue and found that PS1 interacted preferably with proBACE1 rather than mature BACE1. Interestingly, we observed the solid binding between D385A PS1 and proBACE1. Although we cannot clarify a mechanism how D385A PS1 downregulates BACE1 maturation despite the solid interaction in the present study, one explanation is that the transport of proBACE1 to the Golgi after the interaction in the ER can be a process required for BACE1 maturation. We think there is a possibility that D385A PS1 is defective in this trafficking function, although the solid interaction with proBACE1 occurs in the ER. Taken together, PS1 may directly be involved in BACE1 maturation via stabilizing proBACE1 or promoting its efficient transport from the ER to the Golgi, although further experiments are needed to elucidate this mechanism.

In summary, our results show that PS1 is involved significantly in BACE1 maturation. This finding, for the first time, provided us the solid link between β- and γ-secretase. From observations obtained from the present study, we would like to extend our view of PS1 function further, and suggest that PS1 contributes to the dual regulation of β- and γ-secretase by regulating the intracellular trafficking of β-secretase and acting as a key component of γ-secretase. Consequently, PS1 may determine the magnitude of amyloidogenic processing of APP, thereby

contributing to the amyloid pathology. Although the regulatory mechanisms remain unknown, aberrant trafficking function of PS1 may lead to increased Aβ generation, and may underlie the pathogenesis of AD. In a future study, it will be significant to investigate effects of the clinical PS1 mutations or lipid raft on the novel function of PS1 in the intracellular trafficking of BACE1.

ACKNOWLEDGMENTS

We sincerely thank to Dr. De Strooper and Dr. Saftig for providing wt and PS−/− MEF cell lines. We also thank Dr. Kinoshita for helpful discussions.

REFERENCES

Annaert WG, Esselens C, Baert V, Boeve C, Snellings G, Cupers P, Craessaerts K, De Strooper B. 2001. Interaction with telencephalon and the amyloid precursor protein predicts a ring structure for presenilins. Neuron 32:579–589.

Armogida M, Petit A, Vincent B, Scarzello S, da Costa CA, Checler F. 2001. Endogenous beta-amyloid production in presenilin-deficient embryonic mouse fibroblasts. Nat Cell Biol 3:1030–1033.

Bodendorf U, Fischer F, Bodian D, Multhaup G, Paganetti P. 2001. A splice variant of beta-secretase deficient in the amyloidogenic processing of the amyloid precursor protein. J Biol Chem 276:12019–12023.

Borchelt DR, Thinakaran G, Eckman CB, Lee MK, Davenport F, Ratovitsky T, Prada CM, Kim G, Seekins S, Yager D, Slunt HH, Wang R, Seeger M, Levey AI, Gandy SE, Copeland NG, Jenkins NA, Price DL, Younkin SG, Sisodia SS. 1996. Familial Alzheimer's disease-linked presenilin 1 variants elevate Abeta1-42/1-40 ratio in vitro and in vivo. Neuron 17:1005–1013.

Bradford MM. 1976. A rapid and sensitive method for the quantitation of microgram quantities of protein utilizing the principle of protein-dye binding. Anal Biochem 72:248–254.

Cai D, Leem JY, Greenfield JP, Wang P, Kim BS, Wang R, Lopes KO, Kim SH, Zheng H, Greengard P, Sisodia SS, Thinakaran G, Xu H. 2003. Presenilin-1 regulates intracellular trafficking and cell surface delivery of beta-amyloid precursor protein. J Biol Chem 278:3446–3454.

Capell A, Grunberg J, Pesold B, Diehlmann A, Citron M, Nixon R, Beyreuther K, Selkoe DJ, Haass C. 1998. The proteolytic fragments of the Alzheimer's disease-associated presenilin-1 form heterodimers and occur as a 100-150-kDa molecular mass complex. J Biol Chem 273: 3205–3211.

Capell A, Steiner H, Willem M, Kaiser H, Meyer C, Walter J, Lammich S, Multhaup G, Haass C. 2000. Maturation and pro-peptide cleavage of beta-secretase. J Biol Chem 275:30849–30854.

Cordy JM, Hussain I, Dingwall C, Hooper NM, Turner AJ. 2003. Exclusively targeting beta-secretase to lipid rafts by GPI-anchor addition up-regulates beta-site processing of the amyloid precursor protein. Proc Natl Acad Sci U S A 100:11735–11740.

Creemers JW, Ines Dominguez D, Plets E, Serneels L, Taylor NA, Multhaup G, Craessaerts K, Annaert W, De Strooper B. 2001. Processing of beta-secretase by furin and other members of the proprotein convertase family. J Biol Chem 276:4211–4217.

Duff K, Eckman C, Zehr C, Yu X, Prada CM, Perez-tur J, Hutton M, Buee L, Harigaya Y, Yager D, Morgan D, Gordon MN, Holcomb L, Refolo L, Zenk B, Hardy J, Younkin S. 1996. Increased amyloid-beta42(43) in brains of mice expressing mutant presenilin 1. Nature 383: 710–713.

Edbauer D, Winkler E, Haass C, Steiner H. 2002. Presenilin and nicastrin regulate each other and determine amyloid beta-peptide production via complex formation. Proc Natl Acad Sci U S A 99:8666–8671.

Francis R, McGrath G, Zhang J, Ruddy DA, Sym M, Apfeld J, Nicoll M, Maxwell M, Hai B, Ellis MC, Parks AL, Xu W, Li J, Gurney M, Myers RL, Himes CS, Hiebsch R, Ruble C, Nye JS, Curtis D. 2002. aph-1 and pen-2 are required for Notch pathway signaling, gamma-secretase cleavage of betaAPP, and presenilin protein accumulation. Dev Cell 3:85–97.

Fukumoto H, Cheung BS, Hyman BT, Irizarry MC. 2002. Beta-secretase protein and activity are increased in the neocortex in Alzheimer disease. Arch Neurol 59:1381–1389.

Gething MJ. 1999. Role and regulation of the ER chaperone BiP. Semin Cell Dev Biol 10:465–72.

Golde TE, Cai XD, Shoji M, Younkin SG. 1993. Production of amyloid beta protein from normal amyloid beta-protein precursor (beta APP) and the mutated beta APPS linked to familial Alzheimer's disease. Ann N Y Acad Sci 695:103–108.

Gu Y, Chen F, Sanjo N, Kawarai T, Hasegawa H, Duthie M, Li W, Ruan X, Luthra A, Mount HT, Tandon A, Fraser PE, St George-Hyslop P. 2003. APH-1 interacts with mature and immature forms of presenilins and nicastrin and may play a role in maturation of presenilin:nicastrin complexes. J Biol Chem 278:7374–7380.

Haass C, Hung AY, Schlossmacher MG, Oltersdorf T, Teplow DB, Selkoe DJ. 1993. Normal cellular processing of the beta-amyloid precursor protein results in the secretion of the amyloid beta peptide and related molecules. Ann N Y Acad Sci 695:109–116.

Haniu M, Denis P, Young Y, Mendiaz EA, Fuller J, Hui JO, Bennett BD, Kahn S, Ross S, Burgess T, Katta V, Rogers G, Vassar R, Citron M. 2000. Characterization of Alzheimer's beta-secretase protein BACE. A pepsin family member with unusual properties. J Biol Chem 275:21099–21106.

Hardy J. 1997a. The Alzheimer family of diseases: many etiologies, one pathogenesis? Proc Natl Acad Sci U S A 94:2095–2097.

Hardy J. 1997b. Amyloid, the presenilins and Alzheimer's disease. Trends Neurosci 20:154–159.

Hattori C, Asai M, Oma Y, Kino Y, Sasagawa N, Saido TC, Maruyama K, Ishiura S. 2002. BACE1 interacts with nicastrin. Biochem Biophys Res Commun 293:1228–1232.

Hebert SS, Bourdages V, Godin C, Ferland M, Carreau M, Levesque G. 2003. Presenilin-1 interacts directly with the beta-site amyloid protein precursor cleaving enzyme (BACE1). Neurobiol Dis 13:238–245.

Herreman A, Hartmann D, Annaert W, Saftig P, Craessaerts K, Serneels L, Umans L, Schrijvers V, Checler F, Vanderstichele H, Baekelandt V, Dressel R, Cupers P, Huylebroeck D, Zwijsen A, Van Leuven F, De Strooper B. 1999. Presenilin 2 deficiency causes a mild pulmonary phenotype and no changes in amyloid precursor protein processing but enhances the embryonic lethal phenotype of presenilin 1 deficiency. Proc Natl Acad Sci U S A 96:11872–11877.

Herreman A, Van Gassen G, Bentahir M, Nyabi O, Craessaerts K, Mueller U, Annaert W, De Strooper B. 2003. gamma-Secretase activity requires the presenilin-dependent trafficking of nicastrin through the Golgi apparatus but not its complex glycosylation. J Cell Sci 116:1127–1136.

Holsinger RM, McLean CA, Beyreuther K, Masters CL, Evin G. 2002. Increased expression of the amyloid precursor beta-secretase in Alzheimer's disease. Ann Neurol 51:783–786.

Huse JT, Pijak DS, Leslie GJ, Lee VM, Doms RW. 2000. Maturation and endosomal targeting of beta-site amyloid precursor protein-cleaving enzyme. The Alzheimer's disease beta-secretase. J Biol Chem 275:33729–33737.

Hussain I, Powell D, Howlett DR, Tew DG, Meek TD, Chapman C, Gloger IS, Murphy KE, Southan CD, Ryan DM, Smith TS, Simmons DL, Walsh FS, Dingwall C, Christie G. 1999. Identification of a novel aspartic protease (Asp 2) as beta-secretase. Mol Cell Neurosci 14:419–427.

Kamal A, Almenar-Queralt A, LeBlanc JF, Roberts EA, Goldstein LS. 2001. Kinesin-mediated axonal transport of a membrane compartment containing beta-secretase and presenilin-1 requires APP. Nature 414: 643–648.

Kang J, Lemaire HG, Unterbeck A, Salbaum JM, Masters CL, Grzeschik KH, Multhaup G, Beyreuther K, Muller-Hill B. 1987. The precursor of Alzheimer's disease amyloid A4 protein resembles a cell-surface receptor. Nature 325:733–736.

Kihara T, Shimohama S, Sawada H, Kimura J, Kume T, Kochiyama H, Maeda T, Akaike A. 1997. Nicotinic receptor stimulation protects neurons against beta-amyloid toxicity. Ann Neurol 42:159–163.

Kim SH, Leem JY, Lah JJ, Slunt HH, Levey AI, Thinakaran G, Sisodia SS. 2001. Multiple effects of aspartate mutant presenilin 1 on the processing and trafficking of amyloid precursor protein. J Biol Chem 276:43343–43350.

L'Hernault SW, Arduengo PM. 1992. Mutation of a putative sperm membrane protein in Caenorhabditis elegans prevents sperm differentiation but not its associated meiotic divisions. J Cell Biol 119:55–68.

Lee SF, Shah S, Li H, Yu C, Han W, Yu G. 2002. Mammalian APH-1 interacts with presenilin and nicastrin and is required for intramembrane proteolysis of amyloid-beta precursor protein and Notch. J Biol Chem 277:45013–45019.

Leem JY, Saura CA, Pietrzik C, Christianson J, Wanamaker C, King LT, Veselits ML, Tomita T, Gasparini L, Iwatsubo T, Xu H, Green WN, Koo EH, Thinakaran G. 2002a. A role for presenilin 1 in regulating the delivery of amyloid precursor protein to the cell surface. Neurobiol Dis 11:64–82.

Leem JY, Vijayan S, Han P, Cai D, Machura M, Lopes KO, Veselits ML, Xu H, Thinakaran G. 2002b. Presenilin 1 is required for maturation and cell surface accumulation of nicastrin. J Biol Chem 277:19236–19240.

Naruse S, Thinakaran G, Luo JJ, Kusiak JW, Tomita T, Iwatsubo T, Qian X, Ginty DD, Price DL, Borchelt DR, Wong PC, Sisodia SS. 1998. Effects of PS1 deficiency on membrane protein trafficking in neurons. Neuron 21:1213–1221.

Pinnix I, Council JE, Roseberry B, Onstead L, Mallender W, Sucic J, Sambamurti K. 2001. Convertases other than furin cleave beta-secretase to its mature form. FASEB J 15:18101812.

Rogaev EI, Sherrington R, Rogaeva EA, Levesque G, Ikeda M, Liang Y, Chi H, Lin C, Holman K, Tsuda T, et al. 1995. Familial Alzheimer's disease in kindreds with missense mutations in a gene on chromosome 1 related to the Alzheimer's disease type 3 gene. Nature 376:775–778.

Russo C, Schettini G, Saido TC, Hulette C, Lippa C, Lannfelt L, Ghetti B, Gambetti P, Tabaton M, Teller JK. 2000. Presenilin-1 mutations in Alzheimer's disease. Nature 405:531–532.

Sherrington R, Rogaev EI, Liang Y, Rogaeva EA, Levesque G, Ikeda M, Chi H, Lin C, Li G, Holman K, et al. 1995. Cloning of a gene bearing missense mutations in early-onset familial Alzheimer's disease. Nature 375:754–760.

Sinha S, Anderson JP, Barbour R, Basi GS, Caccavello R, Davis D, Doan M, Dovey HF, Frigon N, Hong J, Jacobson-Croak K, Jewett N, Keim P, Knops J, Lieberburg I, Power M, Tan H, Tatsuno G, Tung J, Schenk D, Seubert P, Suomensaari SM, Wang S, Walker D, Zhao J, McConlogue L, John V. 1999. Purification and cloning of amyloid precursor protein beta-secretase from human brain. Nature 402:537–540.

Steiner H, Winkler E, Edbauer D, Prokop S, Basset G, Yamasaki A, Kostka M, Haass C. 2002. PEN-2 is an integral component of the gamma-secretase complex required for coordinated expression of presenilin and nicastrin. J Biol Chem 277:39062–39065.

Thinakaran G. 1999. The role of presenilins in Alzheimer's disease. J Clin Invest 104:1321–1327.

Uemura K, Kihara T, Kuzuya A, Okawa K, Nishimoto T, Ninomiya H, Sugimoto H, Kinoshita A, Shimohama S. 2006. Characterization of sequential N-cadherin cleavage by ADAM10 and PS1. Neurosci Lett 402:278–283.

Uemura K, Kitagawa N, Kohno R, Kuzuya A, Kageyama T, Chonabayashi K, Shibasaki H, Shimohama S. 2003a. Presenilin 1 is involved in maturation and trafficking of N-cadherin to the plasma membrane. J Neurosci Res 74:184–191.

Uemura K, Kitagawa N, Kohno R, Kuzuya A, Kageyama T, Shibasaki H, Shimohama S. 2003b. Presenilin 1 mediates retinoic acid-induced differentiation of SH-SY5Y cells through facilitation of Wnt signaling. J Neurosci Res 73:166–175.

Vassar R, Bennett BD, Babu-Khan S, Kahn S, Mendiaz EA, Denis P, Teplow DB, Ross S, Amarante P, Loeloff R, Luo Y, Fisher S, Fuller J, Edenson S, Lile J, Jarosinski MA, Biere AL, Curran E, Burgess T, Louis JC, Collins F, Treanor J, Rogers G, Citron M. 1999. Beta-secretase cleavage of Alzheimer's amyloid precursor protein by the transmembrane aspartic protease BACE. Science 286:735–741.

Walter J, Fluhrer R, Hartung B, Willem M, Kaether C, Capell A, Lammich S, Multhaup G, Haass C. 2001. Phosphorylation regulates intracellular trafficking of beta-secretase. J Biol Chem 276:14634–14641.

Wilson CA, Doms RW, Zheng H, Lee VM. 2002. Presenilins are not required for A beta 42 production in the early secretory pathway. Nat Neurosci 5:849–855.

Wolfe MS, De Los Angeles J, Miller DD, Xia W, Selkoe DJ. 1999a. Are presenilins intramembrane-cleaving proteases? Implications for the molecular mechanism of Alzheimer's disease. Biochemistry 38:11223–11230.

Wolfe MS, Xia W, Ostaszewski BL, Diehl TS, Kimberly WT, Selkoe DJ. 1999b. Two transmembrane aspartates in presenilin-1 required for presenilin endoproteolysis and gamma-secretase activity. Nature 398:513–517.

Yan R, Bienkowski MJ, Shuck ME, Miao H, Tory MC, Pauley AM, Brashier JR, Stratman NC, Mathews WR, Buhl AE, Carter DB, Tomasselli AG, Parodi LA, Heinrikson RL, Gurney ME. 1999. Membrane-anchored aspartyl protease with Alzheimer's disease beta-secretase activity. Nature 402:533–537.

Yang LB, Lindholm K, Yan R, Citron M, Xia W, Yang XL, Beach T, Sue L, Wong P, Price D, Li R, Shen Y. 2003. Elevated beta-secretase expression and enzymatic activity detected in sporadic Alzheimer disease. Nat Med 9:3–4.

Yu G, Nishimura M, Arawaka S, Levitan D, Zhang L, Tandon A, Song YQ, Rogaeva E, Chen F, Kawarai T, Supala A, Levesque L, Yu H, Yang DS, Holmes E, Milman P, Liang Y, Zhang DM, Xu DH, Sato C, Rogaev E, Smith M, Janus C, Zhang Y, Aebersold R, Farrer LS, Sorbi S, Bruni A, Fraser P, St George-Hyslop P. 2000. Nicastrin modulates presenilin-mediated notch/glp-1 signal transduction and betaAPP processing. Nature 407:48–54.

Human Molecular Genetics, 2007, Vol. 16, No. 1 **50–60**
doi:10.1093/hmg/ddl439
Advance Access published on November 20, 2006

Pael receptor induces death of dopaminergic neurons in the substantia nigra via endoplasmic reticulum stress and dopamine toxicity, which is enhanced under condition of parkin inactivation

Yasuko Kitao[1,*,†], Yuzuru Imai[2,†], Kentaro Ozawa[1], Ayane Kataoka[2], Toshio Ikeda[3], Mariko Soda[2], Kazuhiko Nakimawa[4], Hiroshi Kiyama[4], David M. Stern[7], Osamu Hori[1], Kazumasa Wakamatsu[6], Shosuke Ito[6], Shigeyoshi Itohara[3], Ryosuke Takahashi[2,5,†] and Satoshi Ogawa[1,†]

[1]Department of Neuroanatomy, Kanazawa University Medical School, 13-1, Takara-machi, Kanazawa City, 920-8640 Ishikawa, Japan, [2]Laboratory for Motor System Neurodegeneration and [3]Laboratory for Behavioral Genetics and RIKEN Brain Science Institute (BSI), Saitama 351-0198, Japan, [4]Department of Anatomy and Neurobiology, Osaka City University, Graduate School of Medicine, Osaka, Japan, [5]Department of Neurology, Kyoto University Medical School, Kyoto, Japan, [6]Department of Chemistry, Fujita Health University School of Health Sciences, Aichi 470-1192, Japan and [7]Dean's Office, College of Medicine, University of Cincinnati, Cincinnati, OH 45267, USA

Received August 2, 2006; Revised October 19, 2006; Accepted November 13, 2006

Selective loss of dopaminergic neurons is the final common pathway in Parkinson's disease. Expression of Parkin associated endothelin-receptor like receptor (Pael-R) in mouse brain was achieved by injecting adenoviral vectors carrying a modified neuron-specific promoter and Cre recombinase into the striatum. Upregulation of Pael-R in the substantia nigra pars compacta of mice by retrograde infection induced endoplasmic reticulum (ER) stress leads to death of dopaminergic neurons. The role of ER stress in dopaminergic neuronal vulnerability was highlighted by their decreased survival in mice deficient in the ubiquitin-protein ligase Parkin and the ER chaperone ORP150 (150 kDa oxygen-regulated protein). Dopamine-related toxicity was also a key factor, as a dopamine synthesis inhibitor blocked neuronal death in parkin null mice. These data suggest a model in which ER- and dopamine-related stress are major contributors to decreased viability of dopaminergic neurons in a setting relevant to Parkinson's disease.

INTRODUCTION

Though Parkinson's disease (PD) is a major contributor to disability and death in the aging population, the molecular basis of selective dopaminergic neuronal toxicity is still under investigation. Progression of the clinical syndrome associated with PD, which includes a well-characterized movement disorder, correlates closely with inexorable loss of neurons in the substantia nigra pars compacta (SNpc) (1).

Mutations in the *Parkin* gene (2) have been identified in the autosomal recessive form of PD (AR-JP), a major cause of juvenile PD. Parkin is a 465 amino acid polypeptide with properties of an ubiquitin-protein ligase (E3) whose N-terminus displays homology to ubiquitin and C-terminus is comprised of two RING fingers flanking a cysteine-rich domain, termed in between RING fingers (IBR) (3–5). Consistent with this view, AR-JP-linked parkin mutants are defective in E3 activity (6–8).

A putative G protein-coupled transmembrane polypeptide, Pael Receptor [Parkin-associated endothelin-receptor like receptor (Pael-R)], has been identified as a Parkin substrate (9). Expression of Pael-R in cultured cells results in accumulation

*To whom correspondence should be addressed. Tel: +81 762652162; Fax: +81 762344222; Email: kitao@nanat.m.kanazawa-u.ac.jp
†These authors equally contributed to this work.

of unfolded, insoluble and ubiquinated Pael-R in the ER, eventuating in ER stress, as indicated by upregulation of chaperones, such as GRP78/BiP, and subsequent neuronal death (10). Overexpression of Parkin in this *in vitro* model resulted in removal/degradation of accumulated Pael-R and increased cell viability. The relevance of ER stress in the central nervous system to pathologic situations and normal neuronal development is suggested by induction of the unfolded protein response (UPR) in cell stress associated with cerebral ischemia (11,12) and exposure to excitatory amino acids (13), as well as during rapid neuronal growth in the neonatal period (14). Salient features of the UPR include upregulation of ER chaperones, suppression of general translation, and activation of the upiquitin-proteasome pathway.

A key facet of the pathology of PD is limitation of cell loss to dopaminergic neurons, especially in the SNpc. In this context, studies of Pael-R might be especially relevant. Pan-neuronal expression of Pael-R in *Drosophila* brain caused selective, age-dependent degeneration of dopaminergic neurons (10). Thus, increased levels of Pael-R render dopaminergic neurons vulnerable to cell death. In the current study, we have found that increased expression of Pael-R in mice in the SNpc results in neuronal death which is accentuated by suppression of Parkin (in $Parkin^{-/-}$ mice) or an ER chaperone (in $Orp150^{+/-}$ mice). In contrast, a dopamine (DA) synthesis inhibitor had neuroprotective properties in this system. Thus, we propose a unified model for cytotoxicity in PD through which a combination of ER stress and dopamine toxicity, potentially acting in concert with mitochondrial dysfunction, result in an ascending cycle of cellular perturbation and, ultimately, death of dopaminergic neurons.

RESULTS

Retrograde and neuron-specific gene expression by adenoviral vectors in the SNpc

It was essential to develop a system with cell-specific protein expression which could be targeted to the SNpc. For this purpose, we established two adenoviral vectors in which nuclear Cre-recombinase was driven by cell-specific promoters; for neuronal expression, we employed AxS2NPNCre (abbreviated as S2NPNCre) with a modified SCG10 promoter (superior cervical ganglia neural-specific 10 protein), and for glial-specific expression, we utilized AxGFAPNCre (abbreviated as GFAPNCre) with the glial fibrillary acidic protein promoter (Fig. 1A). When either of these adenoviral vectors was co-infected with AxCALNLEGFP (abbreviated as LoxEGFP), specific expression of EGFP occurred in neurons (with S2NPNCre) or astrocytes (with GFAPNCre) in a cell culture system (not shown). *In vivo*expression studies were performed in mice by co-infecting either S2NPNCre with LoxEGFP, or GFAPNCre with LoxEGFP. Spatial limitation of gene expression was achieved by injecting viral vectors into the striatum (Fig. 1B), resulting in expression of EGFP protein in the ipsilateral SNpc (Fig. 1C, top panel). When S2NPNCre was injected with LoxEGFP, expression of EGFP (marking neurons) and tyrosine hydroxylase [TH; marking dopaminergic neurons in the SNpc (15)] overlapped (Fig. 1C; middle set of panels); quantitation of this overlap by image analysis, based on studying multiple fields, confirmed extensive coexpression of EGFP with TH (Fig. 1D). In contrast, there was no overlap of EGFP, following injection of S2NPNCre with LoxEGFP, when immunostaining was performed to visualize GFAP (Fig. 1C, lowest set of panels and Fig. 1D). These data indicate that co-infection of the striatum with recombinant adenoviral vectors encoding cell-specific Cre recombinase and EGFP (or other transgenes) flanked by lox P sites, leads to retrograde transport of adenovirus in the nigrostriatal system resulting in gene expression in the SNpc.

Expression of Pael-R in the SNpc activates the unfolded protein response

Using this adenoviral system, we sought to express Pael-R in the SNpc. For this purpose, an adenoviral vector was made with expression of Pael-R under control of the SCG10 promoter regulated by the LoxP system (16), AxCALNLPael-R (abbreviated as LoxPael-R; Fig. 2A). Co-injection of the two adenoviral vectors, S2NPNCre and LoxPael-R, into the striatum increased expression of Pael-R in the SNpc (Fig. 2B, referred to as ipsilateral side). Enhanced expression of Pael-R required both vectors to be co-injected, and was specific for neurons.

Based on previous *in vitro* findings, increased expression of Pael-R in dopaminergic neurons might result in ER stress and diminished cell viability (9). Control experiments were performed by co-injecting three adenoviral vectors, S2NPNCre, LoxEGFP and LoxLacZ, into the striatum on one side of the brain, referred to as contralateral (Fig. 2C, upper panels). Expression of an ER chaperone, ORP150 (oxygen-regulated protein 150), known to increase with ER stress (11), was assessed in neurons expressing EGFP (Fig. 2C, upper panels). ORP150 levels, assessed by Western blotting, were unchanged in the SNpc following injection of this combination of adenoviral vectors (Fig. 2D, left portion and Fig. 2E, middle panel, open bars). Faint ORP150 staining was demonstrated in multiple cells and a much stronger signal for EGFP was observed (Fig. 2C, upper panels). ORP150 has a putative ATPase domain and protein binding site, suggesting that it may have a chaperone-like role in maintaining ER function under stress [(17), and see below]. In this context, we have demonstrated that overexpression of ORP150 rescues neurons from cell death mediated by ischemia (11,12) and excitatory amino acids (13). When S2NPNCre, LoxEGFP and LoxPael-R were injected into the striatum on the ipsilateral side of the brain (the vectors with LoxLacZ in place of LoxPael-R were injected on the contralateral side), a prominent increase in Pael-R in the SNpc (Fig, 2D, right portion) was accompanied by increased expression of ORP150 (Fig. 2C, lower panels) in Pael-R expressing neuron (labeled with EGFP). Western blotting indicated that increased expression of ER chaperones, GRP78 and ORP150, reached a maximum by 7–12 days after infection (Fig, 2D, right portion). In contrast, there was no increase in these chaperones on the contralateral side (i.e. the side where the LoxPael-R adenoviral vector was replace by a LoxLacZ vector; Fig. 2D and E). Levels of a cytoplasmic chaperone, the 70 kDa heat shock protein, remained unchanged on both sides of the brain (Fig. 2D). These data indicate that co-infection of

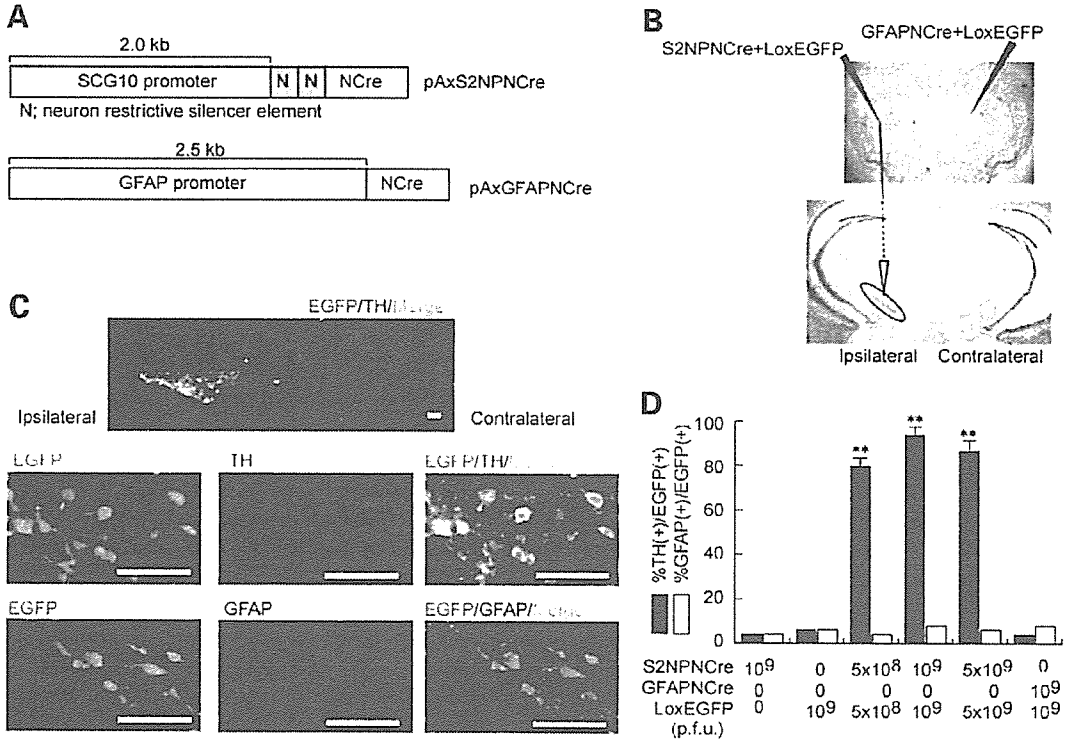

Figure 1. Neuron-specific expression of a transgene in the SNpc after adenoviral infection of the striatum. Two adenoviral vectors were constructed to drive cell type-specific expression of Cre recombinase in neurons (AxS2NPNCre also termed S2NPNCre) and astrocytes (AxGFAPNCre also termed GFAPNCre) (**A**). S2NPNCre was injected unilaterally along with LoxEGFP into the striatum (10^9 p.f.u., in each case) as shown (**B**, upper panel). 7 days after injection, brain slices corresponding to the striatum (B, upper panel) or SNpc (B, lower panel) were analyzed by Nissl staining. On the contralateral side, GFAPNCre was injected along with LoxEGFP (10^9 p.f.u., in each case). SNpc sections were analyzed by fluorescence microscopy using antibodies to TH or GFAP (**C**). Merged images are shown on the top and the far right (marker bar corresponds to 200 μm; note that magnification is greater in the lower panels compared with the top panel), and are representative of six repeat experiments, obtained at −3.1 mM from the Bregma. (**D**) Combinations of adenoviral vectors at the indicated concentrations were injected into the striatum of wild-type mice, and, 7 days later, animals were sacrificed and sections of SNpc were analyzed at five different levels (−3.16, −3.28, −3.40, −3.52 and −3.64 mM from the Bregma). Sections were subjected to image analysis in order to determine the area of TH-positivity [TH(+)] as a percentage of the area of EGFP-positivity [%TH(+)/EGFP(+)]. The mean ± SD is shown ($n = 6$), and ** denotes $P < 0.01$, compared to S2NPNCre infection alone.

LoxPael-R and S2NPNCre in the striatum caused expression of Pael-R in SNpc neurons, and triggered the ER stress.

Expression of Pael-R in SNpc of parkin$^{-/-}$ mice resulted in neuronal death

Parkin null mice (*Parkin*$^{-/-}$) were generated by replacing the proximal exon 3 with a neo cassette (PGK-neo) and two lox P sites (Supplementary Material, Fig. S1A). Southern blotting revealed homologous recombination of the mutant allele (Supplementary Material, Fig. S1B). Reverse transcriptase–polymerase chain reaction (RT–PCR) to detect Parkin transcripts confirmed the absence of normal transcripts in homozygous mutant mice (Supplementary Material, Fig. S1C). Sequencing of RT–PCR products confirmed complete deletion of exon 3 and a frame-shift downstream of exon 2 in mutant mice (Supplementary Material, Fig. S1D). Consistent with these data, western blotting with anti-Parkin antibodies showed the absence of Parkin antigen in brain samples (Supplementary Material, Fig. S1E). Parkin homozygous mutant mice were born at the expected mendelian ratio, showed no overt abnormalities (except a slight decrease in body weight) and had normal lifespans (18,19). Moreover, *Parkin*$^{-/-}$ mice were comparable, in terms of the number of TH-positive neurons in the SNpc, compared to wild-type littermates. However, *Parkin*$^{-/-}$ animals displayed a slight increase in striatal dopamine content, compared with wild-type littermates (not shown).

Parkin has been shown to ubiquinate Pael-R, thereby promoting degradation of insoluble and toxic Pael-R overexpressed in cell culture systems (6). Thus, we hypothesized that similar overexpression of Pael-R in *Parkin*$^{-/-}$ mice might result in severe ER stress and cell death in the SNpc. Using *Parkin*$^{+/+}$ and *Parkin*$^{-/-}$ mice, LoxPael-R was co-injected unilaterally into the striatum with LoxEGFP (as a neuronal marker) and S2NPNCre. Whereas up-regulation of Pael-R was confirmed by immunohistochemical analysis in the ipsilateral SNpc of both types of mice (white arrowheads in the lower panels of Fig. 3A indicate neurons positive with both TH and Pael-R), a marked decrease in the number of Nissl-positive neurons was demonstrated in *Parkin*$^{-/-}$ mice, (Fig. 3A and B). Neurodegeneration in the SNpc was accompanied by loss of TH immunointensity and decreased dopamine content in the striatum (Fig. 3C and D).

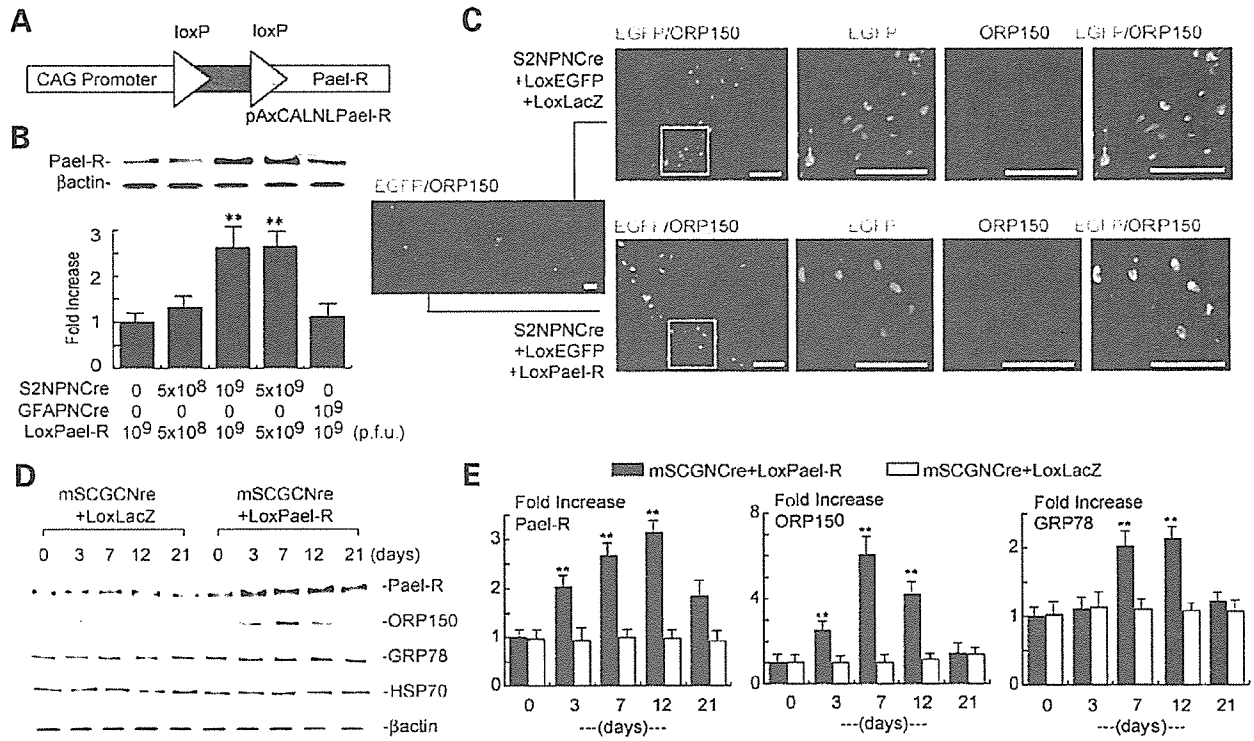

Figure 2. Transfection of Pael-R induces the ER stress in the SNpc. (**A**) Schematic depiction of the construct pAxCALNLPael-R to yield the adenoviral vector AxCALNLPael-R (LoxPael-R). A stuffer sequence (gray box) flanked by two lox-P sequences (arrowhead) was inserted between the promoter and *Pael-R* gene. (**B**) Adenoviral vectors carrying either S2NPNCre, GFAPCre or LoxPael-R were injected into the striatum as described in Figure 1, and, 7 days later, expression of Pael-R was assessed by Western blotting (upper panel), together with the levels of ß-actin as an internal control. Intensity of the corresponding bands was semi-quantitatively assessed by densitometric analysis and expressed in terms of fold-increase versus control samples where no adenovirus was injected (lower panel; $n = 6$, mean ± SD, and ** denotes $P < 0.05$ compared to LoxPael-R infection alone). (**C**) A mixture (total 2 μl) of adenoviral vectors including S2NPNCre (10^9 p.f.u.), LoxEGFP (5×10^8 p.f.u.), and AxCALNLNZ (LoxLacZ; 10^9 p.f.u.) was injected unilaterally in the striatum of C57Black/6J mice (upper panels). The same mixture was injected on the contralateral side, except that LoxLacZ was replaced by LoxPael-R (10^9 p.f.u.; lower panels). Seven days later, animals were perfusion-fixed and brainstem sections were immunostained using anti-ORP150 antibody (red). Merged images with EGFP signals (green) are shown in yellow. Open boxes indicated in the far left panels are magnified in the three panels on the right. Images are representative of six repeat experiments and the marker bar indicates 200 μm. (**D**) S2NPNCre + LoxLacZ (10^9 p.f.u., each) were injected unilaterally (termed ipsilateral) into the striatum, and S2NPNCre + LoxPael-R (10^9 p.f.u., each) were injected on the contralateral side. At the indicated time points, the brainstem was removed. The SNpc was separated and Western blotting was performed using antibodies to ORP150, GRP78, HSP70 and β-actin (images are representative of six repeat experiments). (**E**) Expression of Pael-R (left panel), ORP150 (middle panel), and GRP78 (right panel) on the ipsilateral (open bars) or contralateral side (closed bars) was assessed by densitometric analysis and is expressed as fold-increase versus control (day 0 indicates the day of the operation without injection of adenoviral vectors ($n = 6$, mean ± S.D is shown). ** denotes $P < 0.05$ by multiple comparison analysis compared to day 0 on the ipsilateral side.

No significant neuronal damage was observed in *Parkin*$^{+/+}$ mice after the overexpression of Pael-R using these methods.

To determine whether loss of TH staining in the SNpc, associated with increased expression of Pael-R, was due to neuronal death, we performed TUNEL analysis and monitored expression of a neo-epitope for activated caspase-3 (20). Increased expression of Pael-R in the SNpc, achieved as above (by unilateral injection of S2NPNCre, LoxPael-R and LoxEGFP; the contralateral side was injected with S2NPNCre, LoxLacZ and LoxEGFP as a control), demonstrated a small increase in DNA fragmentation even in the ipsilateral SNpc of wild-type mice (Fig. 4A and C). Increased DNA fragmentation was more striking in the ipsilateral SNpc of *Parkin*$^{-/-}$ mice, with maximal intensity 7 days after infection (Fig. 4B and C). The number of EGFP-and TUNEL-positive cells is significantly increased in the SNpc of *Parkin*$^{-/-}$ mice (Fig. 4B and C). It should be noted that there was a small increase in TUNEL staining on the contralateral side (Fig. 4C) observed most consistently in caudal sections (−3.4 and −3.6 from the Bregma). This might be due, at least in part, to crossed projections from the striatum to the contralateral SNpc. Pilot studies showed EGFP expression in the contralateral SNpc after unilateral injection of S2NPNCre and LoxEGFP, though this was <5% of the EGFP expression observed in the ipsilateral SNpc (not shown). Increased expression of Pael-R in the SNpc, achieved as above, demonstrated a small increase in the intensity of activated caspase-3 staining in the ipsilateral SNpc of wild-type mice (Fig. 4A and D). Expression of activated caspase-3 antigen was more striking in the ipsilateral SNpc of *Parkin*$^{-/-}$ mice (Fig. 4B and D), with maximal intensity 5 days after infection (not shown). The number of EGFP-positive cells costaining with activated caspase-3 is significantly increased in the SNpc of *Parkin*$^{-/-}$ mice (Fig. 4B and D).

Since there was no apparent damage, due to experimental manipulation or other factors, in the ipsilateral striatum (this

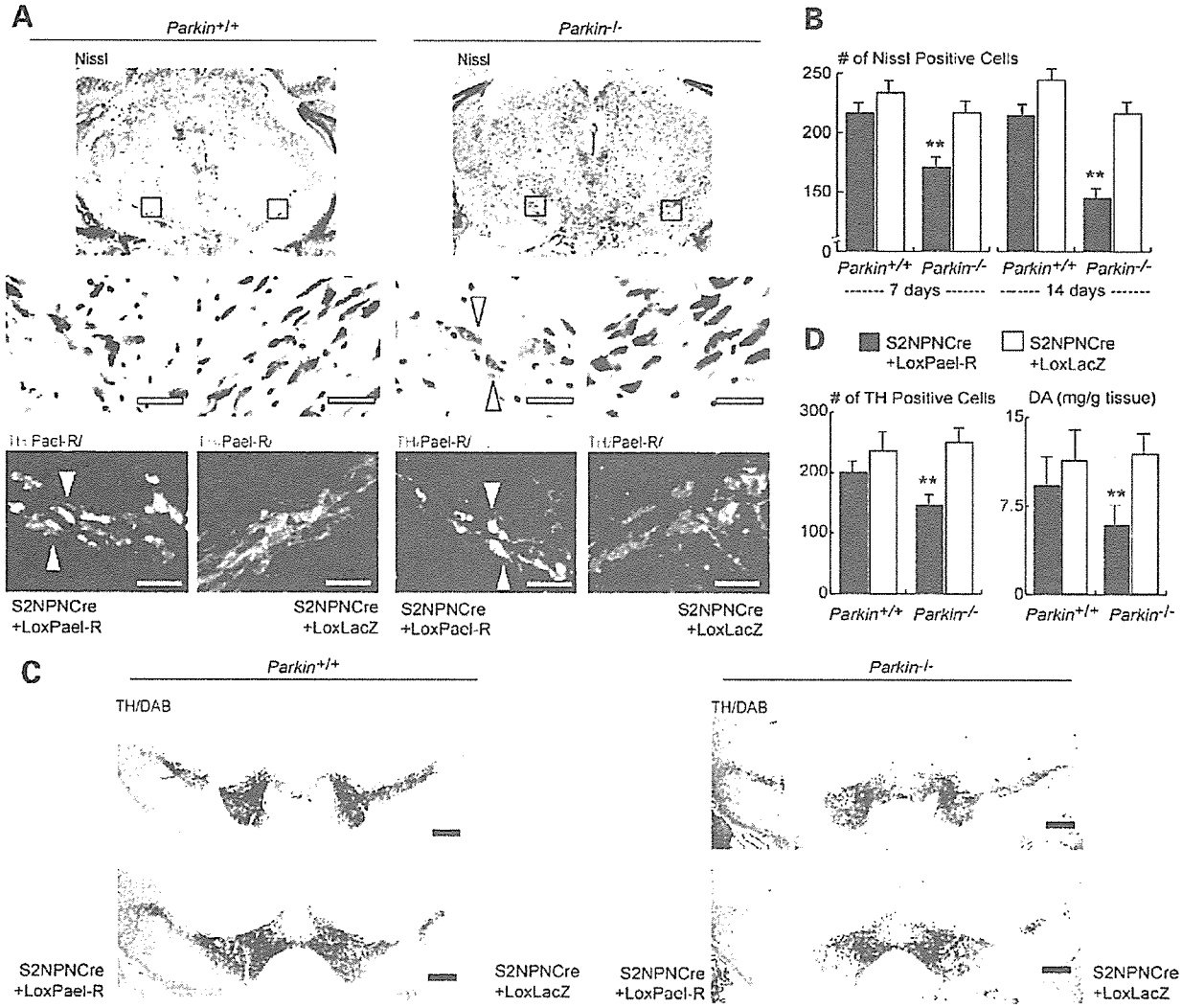

Figure 3. Enhanced neuronal death in the SNpc of parkin$^{-/-}$ mice by the up-regulation of Pael-R. (**A**) Adenoviral vectors (2 μl), including LoxEGFP (5×10^8 p.f.u.), S2NPNCre (10^9 p.f.u.) and LoxPael-R (10^9 p.f.u.) were injected unilaterally in the striatum of either parkin$^{+/+}$ or parkin$^{-/-}$ mice, as described in Figure 1. As a control, LoxPael-R was replaced by LoxLacZ (10^9 p.f.u.), and S2NPNCre + LoxLacZ was injected on the contralateral side. Brains of animals were then perfusion-fixed 7 days later, and midbrain sections were stained using the Nissl method (upper two panels). One of consecutive sections was also immunostained with anti-Pael-R antibody (lower panels). Images at −3.52 mM from the Bregma are shown. The open boxes in the upper panel are magnified in lower two panels. Typical examples of neurons positive with both TH and Pael-R are indicated by white arrowheads in the lower panels. Typical examples of degenerating neurons are identified by the open arrowheads in the middle panels. (**B**) Nissl positive neurons were counted on the ipsilateral (closed bars) and contralateral sides (open bars) as described in the text, 7 and 14 days after the injection. In each case, $n = 6$, and the mean ± SD is shown. ** denotes $P < 0.01$ compared to parkin$^{+/+}$ mice injected with LoxLacZ. (**C**) 10 days after the injection, midbrain sections were stained with anti-TH antibody as described in text. Images at −3.28 mM (upper panels) and −3.52 mM from the Bregma (lower panels) are shown. (**D**) TH positive neurons were counted 7 days after the injection (left panel). DA content was also measured by the HPLC-EC method 7 days after the injection (right panel). In each case, closed and open bars correspond to the ipsilateral (closed bars) or contralateral striatum (open bars) of parkin$^{-/-}$ or parkin$^{+/+}$ mice, respectively. In each case, $n = 6$, and the mean ± SD is shown. ** denotes $P < 0.01$ compared to parkin$^{+/+}$ mice injected with LoxLacZ.

side received injection of S2NPNCre, LoxPael-R and LoxEGFP) based on EGFP fluorescence or Nissl staining (Supplementary Material, Fig. S2B), diminished dopamine content most likely reflects loss of functional dopaminergic neurons in the ipsilateral SNpc. Moreover, injection of S2NPNCre and LoxPael-R resulted in the expression of Pael-R (marked by expression of EGFP) also in the motor cortex by retrograde infection (Supplementary Material, Fig. S2A). In contrast to the SNpc, no neuronal death was observed in either motor cortex or striatum (Supplementary Material, Fig. S2C). In other brain sublesions which have the connection to the striatum (i.e. the thalamus, the interpeduncular nucleus, the locus coeruleus and the raphe nucleus), no EGFP signals were detected, which may be due to the fewer communication to the striatum (not shown). The loss of TH immunointensity in the SNpc mainly occurred in neurons expressing Pael-R (Supplementary Material, Fig. S3A–C). These data suggest that Pael-R overexpression caused neuronal cell death, rather selectively in dopaminergic neurons in the SNpc.

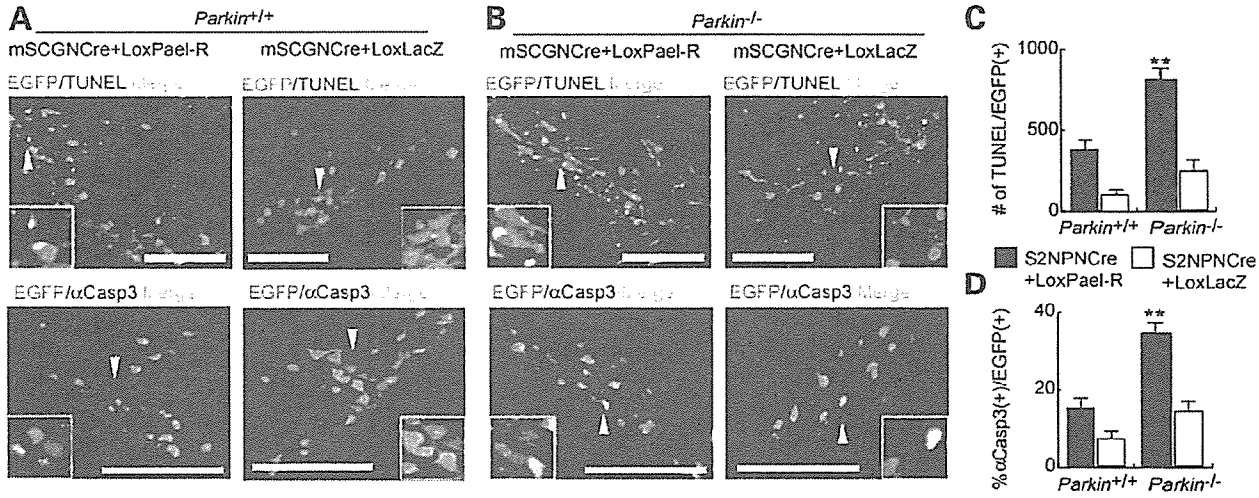

Figure 4. Assessment of neuronal cell death in parkin$^{-/-}$ mice (**A,B**) After infection of adenoviral vectors by the same protocol as used in Figure 3, brains of animals were perfusion-fixed 7 (upper panels for TUNEL) and 5 (lower panels for activated caspase-3 staining) days later, and midbrain sections were stained using either the TUNEL method or anti-activated caspase-3 antibody (αCasp3). Images at −3.52 mM from the Bregma were obtained to visualize the indicated antibody and the EGFP signal (green). In each panel, areas indicated by arrowheads are magnified in the insets at the lower corner of the panel. Note that TUNEL-positive and activated caspase-3-positive cells are increased in the EGFP positive area. Scale bar: 200 μm. Images shown in this figure (panels A,B) are representative of six repeated experiments. (**C,D**) Quantitation of TUNEL-positive signals (number of positive signals) 7 days after injection (panel C) or the percentage of cells positive for activated caspase-3 (αCasp3) in the population of EGFP-positive neurons 5 days after injection (panel D) on the ipsilateral (closed bars) or contralateral SNpc (open bars) of either parkin$^{-/-}$ or parkin$^{+/+}$ mice. In each case, $n = 6$, and the mean ± SD is shown. ** denotes $P < 0.01$ compared to parkin$^{+/+}$ mice injected with LoxLacZ.

ORP150 suppresses Pael-R-mediated neuronal cell death

These observations led us to hypothesize that ER stress might trigger loss of dopaminergic neurons due to accumulation of toxic Pael-R. To gain further insight into mechanisms underlying this observation, we focused on the function of an ER chaperone, ORP150, which promotes protein folding/degradation (17). We reasoned that if the ER stress is the cause of Pael-R-mediated dopaminergic neuron death, even in the presence of wild-type *Parkin*, decreased levels of ORP150 should accentuate Pael-R-induced neuronal death in the SNpc, whereas overexpression of ORP150 might be protective. Using targeted injection of adenoviral vectors (as above), Pael-R was overexpressed in the SNpc of either heterozygous *Orp150* truncation mutants [*Orp150*$^{+/-}$ mice; note, homozygous *Orp150*$^{-/-}$ mice have a developmental lethal phenotype 13)], strain-matched controls (*Orp150*$^{+/+}$ mice) or *Orp150* overexpressing wild-type transgenics [*Orp150* TG mice, driven by pCAGGS promoter (21)]. Elevated levels of ORP150 were confirmed in SNpc neurons of *Orp150* TG mice by immunohistochemical analysis (Supplementary Material, Fig. S4 upper panels; levels of ORP150 in strain-matched normal animals are also shown in lower panels). Degeneration of dopaminergic neurons was assessed by TUNEL staining and expression of activated caspase-3 (Fig. 5A and B), since these methods appeared to have adequate sensitivity, as shown in Figure 4. A gene dosage effect was observed; increased levels of ORP150 afforded protection to dopaminergic neurons. *Orp150*$^{+/-}$ mice, with the lowest levels of functional ORP150, displayed exaggerated damage to dopaminergic neurons; TUNEL staining and activated caspase-3 were enhanced on the ipsilateral SNpc (the side in which injection of adenoviral vectors resulted in over-expression of Pael-R; Fig. 5A and B), whereas no significant cell death was observed on the contralateral side where LoxLacZ was expressed (data not shown). Each of these indices of neuronal stress/toxicity in this setting was decreased, in a manner dependent on the 'dose' of *Orp150*, when the same experiment was performed in wild-type (*Orp150*$^{+/+}$) or mice overexpressing ORP150 (*Orp150* TG mice) (Fig. 5A and B).

These data suggest an essential contribution of ER function in protecting neurons from lethal toxicity when Pael-R is overexpressed. According to this concept, we further reasoned that such neurons in *Parkin*$^{-/-}$ mice might be rescued by either expression of Parkin or ER chaperones capable of promoting protein folding/renaturation, such as GRP78. Though adenoviral expression of LacZ in neurons failed to rescue SNpc neurons from Pael-R-mediated cell death, overexpression of Parkin minimized neuronal damage (Fig. 5C). Similarly, overexpression of GRP78 could substitute for Parkin in preventing Pael-R-mediated neuronal death in *Parkin*$^{-/-}$ mice. Western blot analysis of brain stem samples confirmed the expression of transfected gene products (Fig. 5C, right panel). These data indicate that the ER chaperones, such as GRP78 and ORP150, have the capacity to relieve ER stress due to increased expression of Pael-R, thereby exerting a protective effect on dopaminergic neurons in the SNpc.

Suppression of Pael-R-mediated cell death by inhibition of dopamine synthesis

Increased dopamine content in the striatum of *Parkin*$^{-/-}$ mice has been noted by some investigators, though the increase is small (18,19). Furthermore, Pael-R has been implicated in

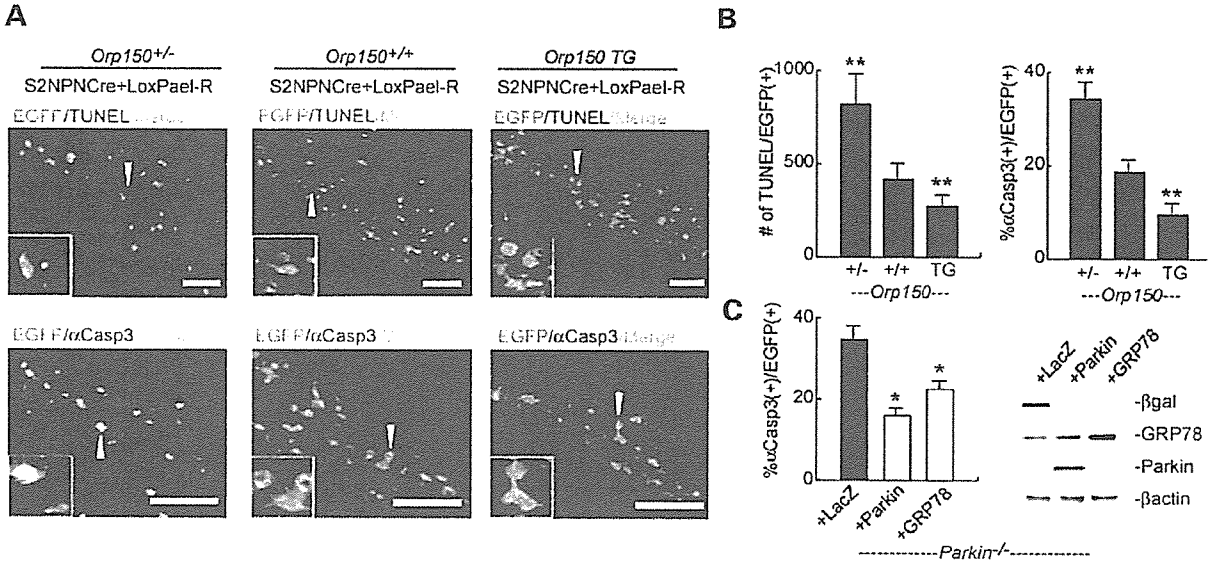

Figure 5. Effect of ORP150, Parkin, and GRP78 on Pael-R-mediated cell death in the SNpc. (**A**) Adenoviral vectors (2 μl), including LoxEGFP (5×10^8 p.f.u.), S2NPNCre (10^9 p.f.u.), and LoxPael-R (10^9 p.f.u.), were injected unilaterally into the striatum of either ORP150$^{+/-}$ (left panels), ORP150$^{+/+}$ (middle panels) or ORP150 transgenic mice (ORP150 TG; right panels) mice. Where indicated, LoxPael-R was replaced with LoxLacZ (10^9 p.f.u.), and the latter mixture was injected on the contralateral side. Brains were then perfusion fixed at 7 (for TUNEL analysis; upper panels) and 5 (for activated caspase-3 staining; αCasp3, lower panels) days after the injection. Images were overlapped with the EGFP signal (green). In each panel, the area indicated by the arrowhead is magnified in a small inset in the lower corner. Note the increase in cells staining positively by TUNEL analysis and for activated caspase-3 antigen in the EGFP positive area. This was most apparent in ORP150$^{+/-}$ mice. Scale bar: 200 μm. All images shown in this figure are representative of six repeated experiments. (**B**) Total number of TUNEL-positive signals (left panel) and the percentage of activated caspase-3 (αCasp3) positive cells in the population of EGFP-positive neurons (right panels) determined in the ipsilateral SNpc. In each case, $n = 6$, and the mean ± SD is shown. ** denotes $P < 0.01$ compared to ORP150$^{+/+}$ (wild type) mice. (**C**) A mixture (total 2 μl) of LoxEGFP (5×10^8 p.f.u.), S2NPNCre (10^9 p.f.u.), LoxPael-R (10^9 p.f.u.), and LoxLacZ (1.5×10^9 p.f.u.) was injected unilaterally into the striatum of parkin$^{-/-}$ mice. On the contralateral side, LoxLacZ was replaced with either AxCMParkin (Parkin; 1.5×10^9 p.f.u.) or AxCAGRP78 (GRP78; 1.5×10^9 p.f.u.). Midbrain sections were stained with anti-activated caspase-3 antibody (5 days later). The percentage of activated caspase-3-positive neurons was determined on the ipsilateral (closed bars) and contralateral sides. In the latter case, data is shown following injection of the vector expressing parkin (gray bars) and GRP78 (open bars) are shown. In each case, $n = 6$, and the mean ± S.D is shown. Midbrain samples collected from parkin$^{-/-}$ mice as described in text were also subjected to Western blot analysis using either anti-β-galactosidase, anti-GRP78, anti-Parkin or anti-β-actin antibody (for an internal control). A typical example of five repeated experiments is shown. * denotes $P < 0.01$ compared to the group injected with the vector expressing LacZ.

the regulation of dopamine levels; increased Pael-R is associated with increased dopamine content in the striatum (Imai, Y. *et al.*, manuscript in preparation). Based on these observations, we reasoned that Pael-R-mediated cell death in the SNpc of *Parkin*$^{-/-}$ mice might be associated with elevated levels of dopamine. Since dopamine has considerable potential toxicity (8,22), we further hypothesized that dopamine-derived metabolites/catabolites might contribute to loss of TH-positive (+) neurons. To address this issue directly, we determined whether suppression of DA synthesis by AMPT, a specific inhibitor of TH (15), would have a neuroprotective effect on TH(+) neurons overexpressing Pael-R in the SNpc of *Parkin*$^{-/-}$ mice. Accidental death of mice occurred in ≈4% of animals within 36 h after the first administration of AMPT. This might be due to the shifts of circadian temperature rhythms (23). The systemic toxicity of AMPT was not observed at later phase. Repeated administration of AMPT over a 7 day period lowered dopamine content of the striatum to ≈30% of that observed in untreated controls (Supplementary Material, Fig. S5). Using this protocol of AMPT treatment, adenoviral vectors were injected into the striatum to increase neuronal Pael-R levels in *Parkin*$^{-/-}$ mice. Compared with *Parkin*$^{-/-}$ mice treated with phosphate-buffered saline (PBS), animals receiving AMPT displayed striking neuroprotection. Inhibition of TH in *Parkin*$^{-/-}$ mice overexpressing Pael-R in the SNpc suppressed the number of TUNEL-positive nuclei and generation of activated caspase-3 epitopes, compared with animals treated with PBS alone (Fig. 6A–C). AMPT treatment was also effective in preventing Pael-R-mediated cell death in the SNpc of *Orp150*$^{+/-}$ mice, compared with animals treated with saline (Fig. 6C), suggesting a toxic effect of DA in ER dysfunction. These data suggest that dopamine enhances neurotoxicity associated with overexpression of Pael-R, especially in the absence of Parkin.

DISCUSSION

Our data indicate that *in vivo* overexpression of Pael-R in neurons of the SNpc results in enhanced ER stress, which, especially in a setting with decreased functional Parkin, targets TH-positive neurons for accentuated cytotoxicity. Whereas expression of a protein as difficult to properly fold as Pael-R has been shown to cause ER stress in a range of cell types *in vitro* (9), we believe that cellular vulnerability in this situation is critically exaggerated in dopaminergic neurons *in vivo* due to the superimposed toxicity of dopamine

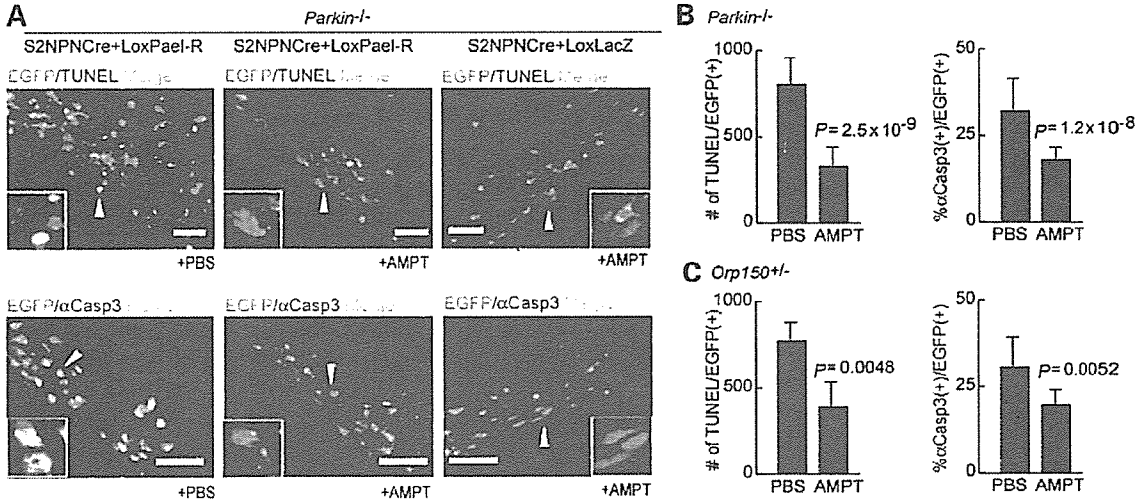

Figure 6. Suppression of neuronal death in the SNpc of mice overexpressing Pael-R by inhibition of dopamine synthetase using AMPT. (**A**) Parkin$^{-/-}$ mice were treated with either PBS or AMPT up to 7 days after unilateral injection of adenoviral vectors, including LoxEGFP (5×10^8 p.f.u.), S2NPNCre (10^9 p.f.u.) and LoxPael-R (10^9 p.f.u.). As a control, the same vectors, with LoxPael-R replaced by LoxLacZ (10^9 p.f.u.), were injected on the contralateral side. Brains were perfusion-fixed at 7 (upper panels; for TUNEL analysis) and 5 (lower panels; staining for activated caspase-3, αCasp3) days after injection of the vectors, and were then subjected to histochemical analysis as described above. The above images were overlapped with EGFP (green). Scale bar: 200 μm. All images shown in this figure are representative of six repetitions of the experimental protocol. In each panel, the area indicated by the arrowhead is magnified in a small inset in the lower corner. Note that TUNEL-positive and activated caspase-3-positive cells were diminished by AMPT treatment (i.e. in the presence of the latter, the area/level of apoptotic cells approximated that observed in controls overexpressing LacZ). (**B,C**) Statistical analysis was performed as described above, in either *Parkin*$^{-/-}$ mice (B) or *Orp150*$^{+/-}$ mice (C). The number of TUNEL-positive signals (left panels), and % of activated caspase-3-positive cells in the population of EGFP-positive neurons (right panels) in the ipsilateral SNpc are shown ($n = 6$; the mean ± SD). *P*-values obtained by Student's t-analysis, are shown in each panel.

(DA) itself. These data also emphasize the potential relevance of parkin targets, such as Pael-R, in addition to the aminoacyl-tRNA synthetase cofactor p38, to neurotoxicity in dopaminergic neurons (24).

The technical approach employed in our experiments, injection of adenovirus under stereotactic guidance into the striatum with selective neuronal expression of gene products, is quite unique. First, such results have been difficult to achieve in the mouse because of anatomic limitations. Though adenovirus vectors are more immunogenic than adenovirus associated virus, they still have greater merits in retrograde transfection (25). We have taken this advantage into our experimental system, to achieve an efficient gene transfer to SNpc, where direct injection of viral vectors will be inapplicable because of anatomical limitations. Second, adenovirus infection predominately affects glia, rather than neurons. Modification of the SCG10 (superior cervical ganglion) promoter by tandem insertion of two neuron-restrictive silencers produced almost 100% expression of transgenes in neuronal cultures, and considerably lower expression in astrocytes (not shown). Coinjection of S2NPNCre with LoxEGFP into the striatum resulted in expression of transgenes in neurons of the mouse SNpc. This approach allowed us to obtain neuron-specific expression of Pael-R enabling study of its effect(s) on neuronal physiology *in vivo*. The proximal result of such Pael-R expression included upregulation of ER chaperones, such as GRP78 and ORP150, whereas the distal result was loss of TH-positive neurons, especially in *Parkin*$^{-/-}$ mice. In contrast, expression of Pael-R had no effect on the constitutively expressed form of HSP70, important for housekeeping functions in the cytoplasm (Fig. 2D).

Several observations are consistent with the importance of ER stress as a mechanism underlying Pael-R-induced cellular toxicity. In previous studies using cultured neuroblastoma cells, Pael-R has been identified as a substrate of Parkin, an E3 ubiquitin ligase (6). Thus, in the absence of Parkin, Pael-R may accumulate since it is not subject to efficient removal. In contrast, no detectable change of Pael-R levels has been reported in SNpc of Parkin null mice (24). Since there is no evidence of progressive neuronal cell death in Parkin null mice, there would appear to be redundant mechanisms able to compensate for loss of Parkin under physiologic conditions. The ability of neurons to withstand ER stress imposed by expression of Pael-R is likely to be dependent on the effectiveness of the ER-stress response; higher levels of Pael-R would require a facile ER-stress response (i.e. adequate or increased levels of parkin, ORP150, GRP78 etc), whereas diminished levels of ORP150 or GRP78 would render neurons vulnerable to toxicity because of a compromised stress response. These predictions have been borne out by our experimental results. Therefore, the possible toxicity of Pael-R cannot be completely ignored, especially in pathological conditions. Increasing expression of GRP78 had a protective effect in *Parkin*$^{-/-}$ mice overexpressing Pael-R. Furthermore, expression of ORP150, an important factor modulating ER stress even in the presence of Parkin, modulated the toxicity of Pael-R for dopaminergic neurons; increased levels of ORP150 in transgenic mice were neuroprotective, whereas diminished levels in ORP150 in *Orp150*$^{+/-}$ mice resulted in enhanced cell death (i.e. increased TUNEL staining and immunoreactivity for activated caspase-3 in the SNpc).

Our experimental system produced Pael-R overexpression and subsequent cell death in the SNpc of mouse, whereas no apparent cell death occurred either in the striatum or in the motor cortex (Supplementary Material, Fig. S2C). Furthermore, we observed a neuroprotective effect of a TH inhibitor in the SNpc of mouse, suggesting that DA also contributes to Pael-R-induced cell death of dopaminergic neurons. Consistent with these results in our mouse models, studies in transgenic flies overexpressing Pael-R in most of neuronal populations also showed selective loss of dopaminergic neurons, though the mechanism of cellular degeneration is not fully understood (10). One plausible explanation for focusing toxicity on dopaminergic neurons is the oxidative stress caused by the presence of DA and its derivatives (1). Another possibility that DA might compromise the survival of dopaminergic neurons is a chemical inactivation of cellular proteins by addition of DA to sulfhydryl group of proteins. Recently, it has been reported that dopamine covalently modifies Parkin, a protein rich in sulfhydryl group, in dopaminergic cells, leading to increased Parkin insolubility and inactivation of its E3 function (22). Vulnerability of Parkin to modification by DA further impairs degradation of Pael-R. Thus, even in sporadic PD, DA might interfere in the degradation of certain proteins, such as Pael-R, by the inactivation of Parkin. Collectively, these data propose a model in which a combination of ER stress and DA-related stress plays an important role in degeneration of dopaminergic neurons in sporadic PD as well as PD caused by *parkin* mutations.

MATERIALS AND METHODS

Targeted disruption of the mouse parkin gene

Parkin$^{-/-}$ mice were generated using standard gene targeting techniques (26). A targeting vector was constructed with a 15.7 kb genomic DNA fragment containing exon 3 of the parkin gene (Supplementary Material, Fig. S1). The region containing exon 3 was replaced with a Floxed pgk-neo cassette. A DT-ApA cassette was flanked at the 5′-end of the homologous arm for negative selection (27). The linearized targeting vector was transfected into E14 (129sv) ES cells. Positive clones were selected by Southern blotting, and then injected into C57Bl/6J (B6) blastocysts. Offspring harboring the targeted allele were generated by crossing chimeric mice with B6 mice. Results of such crosses were confirmed by Southern analysis.

Reverse transcription–polymerase chain reaction analysis of parkin null mice

Total RNA was extracted from whole brain tissue using Isogen (Nippon gene). RT reactions containing 1 μg of total RNA were performed using the SuperScript II First-Strand Synthesis System for RT–PCR (Invitrogen). The resulting cDNA was added to PCR reactions containing 1 unit of Ex *Taq* DNA Polymerase (Takara) for 35 PCR cycles. PCR products were separated on a 1% agarose gel. Primers were as follows: RT primer, 5′-agt ttc cct tga ggt tgt gc; Primer A, 5′-cgt agg tcc ttc tcg acc; Primer B, 5′-ttg agg ttg tgc gtc cag g; Primer C, 5′-acc tca gag ggc tcc ata tg; and, Primer D, 5′-ctc tct cta cac gtc aaa cca gtg.

Construction of adenoviral vectors

Modified SCG10 (S2NP10) promoter [2 kb (28)] and mouse GFAP promoter region (2.5 kb; kindly provided by Dr Ikenaka, National Institute for Physiological Science) were cloned into pAxAwNCre (kindly provided by Dr Saito, Tokyo University), a promoter-less cosmid vector for preparing cell type-specific Cre-recombinase expressing adenovirus (Fig. 2A; AxS2NPNCre and AxGFAPNCre). Human Pael-R (9) was cloned into pAxCALNLw (Takara Bio Inc., Shiga, Japan) in order to control Pael-R expression using Cre recombinase (AxLNLPael-R). The Pael-R gene is silenced because of the presence of the staffer of the neo-resistant gene, and is activated by Cre-mediated excisional deletion of the stuffer when a sufficient amount of Cre recombinase is expressed (Fig. 3). To prepare an adenoviral vector of parkin (AxCMParkin), the human parkin gene was cloned into pAxCMwt. Recombinant adenovirus was generating using the COS-terminal protein complex (TPC) method and the Takara adenovirus expression kit (Takara Bio Inc.). AxLNLNZ (Takara Bio Inc.), which overexpresses LacZ with a nuclear localization signal mediated by Cre recombinase, was used for control experiments. Cre-mediated EGFP-expressing adenovirus, AxLNLEGFP, was kindly provided by Dr Okado (Tokyo Metropolitan Institute of Neuroscience). An adenoviral vector for overexpression of GRP78/Bip (AxCAGRP78) was generously provided by Drs S. Tanaka and T. Koike [(29) Graduate School of Science, Hokkaido University]. Each adenovirus was amplified in HEK293 cells and purified using VIRAPREP Adenovirus Purification Kit (Virapur LLC., San Diego, CA, USA). Viral titers were determined by a plaque-forming assay in HEK293 cells.

Western blotting

Levels of Pael-R in tissue extracts were determined by Western blotting as described (9). Mouse brain was quickly removed and placed on a cold plate. Brain slices (200 μm) were obtained at −3.5 mM from the Bregma on a vibratome. Substantia nigra was then carefully removed under guidance of a stereoscopic microscope according to the mouse brain atlas (Paxinos and Franklin, Academic Press, 1997, San Diego) using the cerebral peduncle and medial lemniscus as landmarks. Tissue extracts were prepared from SNpc in PBS containing NP-40 (1%). Proteins were separated by SDS-PAGE, and transferred to PVDF. PVDF was then incubated with antibody to either human Pael-R or ß-actin, the latter as an internal control (1000 × dilution, Sigma, St Louis, MO, USA). Levels of chaperones in tissue extracts were determined by Western blotting, as described (30). PVDF was incubated with either anti-human ORP150 antibody (1 μg/ml), anti-GRP78 monoclonal antibody (Stressgen, Canada; 0.2 μg/ml), or anti-HSP73 antibody (0.1 μg/ml; Stressgen). Where indicated, either anti-β-galactosideas antibody (1000 × dilution, Sigma) or anti-Parkin antibody (1000 × dilution, Cell Signaling Technologies Inc.) was

used to access the level of these proteins. Images were further subjected to densitometric analysis using NIH image software.

Injection of adenoviral vectors into the striatum and treatment of animals

Animals were housed and treated according to institutional and national guidelines. Mice were stereotactically positioned under deep anesthesia, and the indicated combination of adenovirus vectors was injected unilaterally (a different combination, including a LacZ control, was injected on the contralateral side) into the striatum at six points (AP/ML/DV/ = 0.8/1.2/−2.5, 0.8/1.2/−3.2, 0.8/1.7/−2.5, 0.8/1.7/−3.2, 0.8/2.2/−2.5 and 0.8/2.2/−3.2; units are mm), followed by free access to food and water. Retrograde passage and infection of adenoviruses was confirmed 5–12 days after the injection by detection of a green fluorescent signal in the SNpc by fluorescence microscopy. Where indicated, animals were pretreated with α-methyl-DL-Tyrosine (AMPT) to suppress DA synthesis. AMPT-HCl (150 mg/kg, Sigma) was intra-peritoneally administrated twice per day for 5 days before injection of adenoviral vectors, as well as after the latter and until the day of sacrifice.

Assessment of neuronal death *in vivo*

At the indicated time points, animals were perfused with 4% paraformaldehyde under deep anesthesia, the brain was excised and coronal brain sections (14 μm) were cut on a cryostat. Sections were processed for cresyl violet staining or immunohistochemistry using either mouse anti-tyrosine hydroxylase antibody (TH; 1 μg/ml, Sigma), rabbit anti-human ORP 150 antibody [5 μg/ml (30)], rabbit anti-activated casepase-3 antibody(0.1 μg/ml, Genzyme/Teche), rabbit anti-Pael-R antibody [10 μg/ml, (9)] or goat anti-GFAP antibody (4 μg/ml. Santa Cruz Biotechnology, Santa Cruz, CA). Sections were also subjected to TUNEL staining using a commercially available kit (ApopTag, Intergen, Purchase, NY). To evaluate neuronal death in the SNpc, either Nissl or EGFP positive cells were counted in each coronal slice obtained at five different levels (−3.16, −3.28, −3.40, −3.52 and −3.64 mM from the Bregma), as described (31) by acquiring digital images using a CCD camera (Nikon, Coolscope). Cell death was semi-quantitatively assessed by counting TUNEL-positive cells/nuclei in the EGFP-positive area, and evaluating the percentage of activated caspase-3-positive cells in the population of EGFP-positive cells. Sections were analyzed using a laser scanning confocal microscope system (Leica, TCS SP2). In each case, two observers without knowledge of the experimental protocol evaluated sections and experiments were repeated at least three times.

DA content in the striatum was measured in the SNpc as described (32). In brief, striatal tissue was homogenized in solution H (0.4 M $HClO_4$ containing 4 mM $Na_2S_2O_5$, 4 mM diethylenetriaminepentaacetic acid, and 5 mM 1,4-dithiothreitol). Crude tissue lysate was separated on a C-18 reversed-phase column (MCM HPLC, 4.6 mM × 15 cm, 5 ml, ESA, Chelmsford, MA, USA), followed by electrochemical detection (Coulochem III, ESA).

Statistical analysis

Data shown represent the mean ± SD Multiple group comparisons were performed by one-way ANOVA, followed by Newman-Kuels test as a *post hoc* analysis. Comparison between two groups was analyzed by two-tailed Student's *t*-test.

SUPPLEMENTARY MATERIAL

Supplementary Material is available at HMG Online.

ACKNOWLEDGEMENTS

We thank Dr Martin Hooper (Western General Hospital, Edinburgh) for generous contribution of E14 cell line, and Drs Yumi Onodera, Yoshikazu Saito, Hitomi Suzuki (RIKEN, Wako, Japan) for technical assistance for establishing chimera mice. The authors also appreciate the generous gifts of AxCALNLEGFP, GAG promoter and Ax1CAGRP78 from Drs Haruo Okado (Tokyo Metropolitan Institute for Neuroscience), Jun-Ichi Miyazaki (Osaka University Medical School), and Shuuitsu Tanaka and Tetsuro Koike (Hokkaido University), respectively. This work was partially supported by the Ministry of Education, Science, Sports and Culture, a Grant-in-Aid for Scientific Research on Priority Areas—Advanced Brain Science Project—#15016120 to R.T., for Scientific Research (A) #14207032 to R.T., and for Young Scientists (A) #15680011 to Y.I. and a grant from the Special Postdoctoral Researcher Program of RIKEN to Y.I.

Conflict of Interest statement. None declared.

REFERENCES

1. Blum, D., Torch, S., Lambeng, N., Nissou, M., Benabid, A.L., Sadoul, R. and Verna, J.M. (1999) Molecular pathways involved in the neurotoxicity of 6-OHDA, dopamine and MPTP: contribution to the apoptotic theory in Parkinson's disease. *Trends. Biochem. Sci.*, **24**, 135–172.
2. Kitada, T., Asakawa, S., Hattori, N., Matsumine, H., Yamamura, Y., Minoshima, S., Yokochi, M., Mizuno, Y. and Shimizu, N. (1998) Mutations in the parkin gene cause autosomal recessive juvenile parkinsonism. *Nature*, **392**, 605–608.
3. Morett, E. and Bork, P. (1999) A novel transactivation domain in parkin. *Trends. Biochem. Sci.*, **24**, 229–231.
4. Jackson, P.K., Eldridge, A.G., Freed, E., Furstenthal, L., Hsu, J.Y., Kaiser, B.K. and Reimann, J.D. (2000) The lore of the RINGs: substrate recognition and catalysis by ubiquitin ligases. *Trends. Cell. Biol.*, **10**, 429–439.
5. Takahashi, R., Imai, Y., Hattori, N. and Mizuno, Y. (2003) Parkin and endoplasmic reticulum stress. *Ann. N.Y. Acad. Sci.*, **991**, 101–106.
6. Imai, Y., Soda, M. and Takahashi, R. (2000) Parkin suppresses unfolded protein stress-induced cell death through its E3 ubiquitin-protein ligase activity. *J. Biol. Chem.*, **275**, 35661–36664.
7. Shimura, H., Hattori, N., Kubo, S., Mizuno, Y., Asakawa, S., Minoshima, S., Shimizu, N., Iwai, K., Chiba, T., Tanaka, K. and Suzuki, T. (2000) Familial Parkinson disease gene product, parkin, is a ubiquitin-protein ligase. *Nat. Genet.*, **25**, 302–305.
8. Tanaka, K., Suzuki, T., Hattori, N. and Mizuno, Y. (2004) Ubiquitin, proteasome and parkin. *Biochim. Biophys. Acta.*, **29**, 235–247.
9. Imai, Y., Soda, M., Inoue, H., Hattori, N., Mizuno, Y. and Takahashi, R. (2001) An unfolded putative transmembrane polypeptide, which can lead to endoplasmic reticulum stress, is a substrate of Parkin. *Cell.*, **105**, 891–902.

10. Yang, Y., Nishimura, I., Imai, Y., Takahashi, R. and Lu, B. (2003) Parkin suppresses dopaminergic neuron-selective neurotoxicity induced by Pael-R in drosophila. *Neuron*, **27**, 911–924.
11. Tamatani, M., Matsuyama, T., Yamaguchi, A., Mitsuda, N., Tsukamoto, Y., Taniguchi, T., Che, Y.H., Ozawa, K., Hori, O., Nishimura, H. *et al.* (2001) ORP150 protects against hypoxia/ischemia-induced neuronal death. *Nat. Med.*, **7**, 317–323.
12. Miyazaki, M., Ozawa, K., Hori, O., Kitao, Y., Matsushita, K., Ogawa, S. and Matsuyama, T. (2002) Expression of ORP150 (150 kDa oxygen regulated protein) in the hippocampus suppresses delayed neuronal cell death. *J. Cereb. Blood Flow Metab.*, **22**, 979–987.
13. Kitao, Y., Ozawa, K., Miyazaki, M., Tamatani, M., Kobayashi, T., Yanagi, H., Okabe, M., Ikawa, M., Yamashima, T., Tohyama, M. *et al.* (2001) Expression of 150 kDa Oxygen Regulated Protein (ORP150), a molecular chaperone in the endoplasmic reticulum, rescues hippocampal neurons from glutamate toxicity. *J. Clin. Invest.*, **108**, 1439–1450.
14. Kitao, Y., Hashimoto, K., Matsuyama, T., Iso, H., Tamatani, T., Hori, O., Stern, D.M., Kano, M., Ozawa, K. and Ogawa, S. (2004) ORP150/HSP12A regulates Purkinje cell survival: a role for endoplasmic reticulum stress in cerebellar development. *J Neurosci.*, **24**, 1486–1496.
15. Dong, Z., Ferger, B., Paterna, J.C., Vogel, D., Furler, S., Osinde, M., Feldon, J. and Bueler, H. (2003) Dopamine-dependent neurodegeneration in rats induced by viral vector-mediated overexpression of the parkin target protein, CDCrel-1. *Proc. Natl Acad. Sci. U.S.A.*, **100**, 12438–12443.
16. Kanegae, Y., Lee, G., Sato, Y., Tanaka, M., Nakai, M., Sakaki, T., Sugano, S. and Saito, I. (1995) Efficient gene activation in mammalian cells by using recombinant adenovirus expressing site-specific Cre recombinase. *Nucleic Acids Res.*, **23**, 3816–3821.
17. Bando, Y., Ogawa, S., Yamaguchi, A., Kuwabara, K., Ozawa, K., Hori, O., Yanagi, H., Tamatani, M. and Tohyama, M. (2000) The 150 kDa Oxygen Regulated Protein (ORP150) functions as a novel molecular chaperone in the protein transport of the MDCK cells. *Am. J. Physiol. (Cell Physiol.)*, **278**, C1172–C1182.
18. Itier, J.M., Ibanez, P., Mena, M.A., Abbas, N., Cohen-Salmon, C., Bohme, G.A., Laville, M., Pratt, J., Corti, O., Pradier, L. *et al.* (2003) Parkin gene inactivation alters behaviour and dopamine neurotransmission in the mouse. *Hum. Mol. Genet*, **12**, 2277–2291.
19. Goldberg, M.S., Fleming, S.M., Palacino, J.J., Cepeda, C., Lam, H.A., Bhatnagar, A., Meloni, E.G., Wu, N., Ackerson, L.C., Klapstein, G.J. *et al.* (2003) Parkin-deficient mice exhibit nigrostriatal deficits but not loss of dopaminergic neurons. *J. Biol. Chem*, **278**, 43628–43635.
20. Selimi, F., Doughty, M., Delhaye-Bouchaud, N. and Mariani, J. (2000) Target-related and intrinsic neuronal death in lurcher mutant mice are both mediated by caspaea-3 actvation. *J. Neurosci.*, **20**, 992–1000.
21. Bando, Y., Tsukamoto, Y., Katayama, T., Ozawa, K., Kitao, Y., Hori, O., Stern, D.M., Yamauchi, A. and Ogawa, S. (2004) ORP150/HSP12A protects renal tubular epithelium from ischemia-induced cell death. *FASEB J.*, **18**, 1401–1403.
22. Lavoie, M.J., Ostaszewski, B.L., Weihofen, A., Schlossmacher, M.G. and Selkoe, D.J. (2005) Dopamine covalently modifies and functionally inactivates parkin. *Nat. Med.*, **11**, 1214–1221.
23. Cahill, A.L. and Ehret, C.F. (1982) Alpha-methyl-p-tyrosine shifts circadian temperature rhythms. *Am. J. Physiol.*, **243**, R218–R222.
24. Ko, H.S., vonCoelln, R., Sriram, S.R., Kim, S.W., Chung, K.K., Pletnikova, O., Troncoso, J., Johnson, B., Saffary, R., Goh, E.L. *et al.* (2005) Accumulation of the authentic parkin substrate aminoacyl-tRNA synthetase cofactor, p38/JTV-1, leads to catecholaminergic cell death. *J. Neurosci.*, **25**, 7968–7978.
25. Barkats, M., Bilang-Bleuel, A., Buc-Caron, M.H., Castel-Barthe, M.N., Corti, O., Finiels, F., Horellou, P., Revah, F., Sabate, O. and Mallet, J. (1998) Adenovirus in the brain: recent advances of gene therapy for neurodegenerative diseases. *Prog. Neurobiol.*, **55**, 333–341.
26. Gomi, H., Yokoyama, T., Fujimoto, K., Ikeda, T., Katoh, A., Itoh, T. and Itohara, S. (1995) Mice devoid of the glial fibrillary acidic protein develop normally and are susceptible to scrapie prions. *Neuron*, **14**, 29–41.
27. Yanagawa, Y., Kobayashi, T., Ohnishi, M., Kobayashi, T., Tamura, S., Tsuzuki, T., Sanbo, M., Yagi, T., Tashiro, F. and Miyazaki, J. (1999) Enrichment and efficient screening of ES cells containing a targeted mutation: the use of DT-A gene with the polyadenylation signal as a negative selection maker. *Transgenic Res.*, **8**, 215–221.
28. Namikawa, K., Murakami, K., Okamoto, T., Okado, H. and Kiyama, H. (2006) A newly modified SCG10 promoter and Cre/loxP-mediated gene amplification system achieve highly specific neuronal expression in animal brains. *Gene Ther.*, **13**, 1244–1250.
29. Satoh, T., Furuta, K., Tomokiyo, K., Nakatsuka, D., Tanikawa, M., Nakanishi, M., Miura, M., Tanaka, S., Koike, T., Hatanaka, H. *et al.* (2000) Facilitatory roles of novel compounds designed from cyclopentenone prostaglandins on neurite outgrowth-promoting activities of nerve growth factor. *J. Neurochem.*, **75**, 1092–1102.
30. Kuwabara, K., Matsumoto, M., Ikeda, J., Hori, O., Ogawa, S., Maeda, Y., Kitagawa, K., Imuta, N., Kinoshita, K., Stern, D. *et al.* (1996) Purufication and characterization of a novel stress protein, the 150 kDa oxygen regulated protein (ORP150), from cultured rat astrocytes, and its expression in ischemic mouse brain. *J. Biol. Chem.*, **279**, 5025–5032.
31. Kuhn, K., Wellen, J., Link, N., Maskri, L., Lubbert, H. and Stichel, C.C. (2003) The mouse MPTP model: gene expression changes in dopaminergic neurons. *Eur. J. Neurosci.*, **17**, 1–12.
32. Itoh, S., Katsuura, G. and Takashima, A. (1988) Effect of vasoactive intestinal peptide on dopaminergic system in the rat brain. *Peptides*, **9**, 315–317.